

Frequency-Domain System Identification for Unmanned Helicopters from Flight Data

Mohammadhossein Mohajerani

A Thesis
in
The Department
of
Mechanical and Industrial Engineering

Presented in Partial Fulfillment of the Requirements
for the Degree of Master of Applied Science at
Concordia University
Montréal, Québec, Canada

September 2014

© Mohammadhossein Mohajerani, 2014

CONCORDIA UNIVERSITY

School of Graduate Studies

This is to certify that the thesis proposal prepared

By: **Mohammadhossein Mohajerani**

Entitled: **Frequency-Domain System Identification for Unmanned Helicopters from Flight Data**

and submitted in partial fulfilment of the requirements for the degree of

Master of Applied Science

complies with the regulations of this University and meets the accepted standards with respect to originality and quality.

Signed by the final examining committee:

_____ Dr. I. Contreras
_____ Dr. W. Zhu , Examiner, External
_____ Dr. B. Gordon, Examiner
_____ Dr. Y. Zhang, Supervisor
_____ Dr. H. Bolandhemmat, Supervisor

Approved by _____

Dr. Martin D. Pugh, Chair

Department of Mechanical and Industrial Engineering

Dr. Amir Asif

Dean, Faculty of Engineering and Computer Science

ABSTRACT

Developing accurate and realistic models for Unmanned Aerial Vehicles (UAVs) is a central task in effective controller design, autopilot design, and simulation model validation. System identification methods have been extensively used as reliable and less expensive alternatives for conventional analytical modeling for large-scale aircraft in the past. Yet, there is limited work on the identification of mathematical models for small-scale unmanned helicopters. This thesis focuses on development of a system identification tool for rotary-wing UAVs based on frequency-domain non-parametric and parametric identification methods. The tool, which is designed to be embedded in the computer simulation software available for a UAV platform, employs nonlinear parameter estimation and optimization techniques with the purpose of predicting dominant dynamics of the UAV from measured responses and controls. The real flight data acquired from the testbed have been used for testing and verifying the developed system identification tool. The testbed is a commercially available radio-controlled helicopter, Trex-700, equipped with MP2128G2Heli MicroPilot autopilot, and the flight tests are conducted by MicroPilot in hover regime to excite attitude dynamics of the vehicle. The identification results using the developed tool are validated with CIPHER[®] framework which is a highly reliable tool in aircraft system identification. The results demonstrate excellent prediction capability of the developed tool for model identification of the testing UAV platform.

Dedicated to

My Family

ACKNOWLEDGEMENTS

None of this would have been possible without the love and patience of my family. My father, my mother, and my sister, to whom this thesis is dedicated, have been a constant source of love, concern, support and strength all these years. I would like to express my heart-felt gratitude to my family first.

My deepest gratitude is to my supervisor, Dr. Youmin Zhang. I have been amazingly fortunate to have a supervisor who gave me the freedom to explore on my own, and at the same time the guidance to recover when my steps faltered. His patience and support helped me overcome many crisis situations and finish this thesis. I am grateful to him for holding me to a high research standard and enforcing strict validations for each research result. My co-supervisor, Dr. Hamid Bolandhemmat, has been always there to listen and give advice. I am deeply grateful to him for the long discussions that helped me sort out the technical details of my work. His insightful comments and constructive criticisms at different stages of my research were thought-provoking and they helped me focus my ideas.

I am grateful to my good friend and colleague, Dr. Iman Sadeghzadeh, for his encouragement and practical advice throughout my studies. I am also thankful to MicroPilot flight test crew specifically Mr. Nick Playle for performing flight tests on the helicopter testbed.

Mr. Hossein Babini and Mr. Atabak Sadeghi, my long-time friends and former classmates, deserve a great appreciation. Their support and care helped me overcome setbacks and stay focused on my graduate study. Many friends helped me stay sane through these difficult years. I greatly value their friendship and I deeply appreciate their belief in me.

Finally, I appreciate the financial support from Natural Sciences and Engineering Research Council of Canada (NSERC) and MicroPilot that funded this research.

TABLE OF CONTENTS

LIST OF FIGURES	ix
LIST OF TABLES	xi
1 Introduction	1
1.1 Research Motivation	5
1.2 Thesis Outline	7
2 Flight Experiment	8
2.1 Introduction	8
2.2 Scope of Input Design	10
2.3 Input Detailed Design	16
2.3.1 Piloted Frequency Sweep	17
2.3.2 Doublet Input	19
2.4 Introduction to the UAV Testbed	22
2.5 Flight Test Implementation	23
2.6 Flight Test Results	26
3 Frequency-Response Identification	28
3.1 Introduction	28
3.2 Time-Frequency Transformation	29
3.3 Frequency-Response Function	31
3.3.1 Rough Estimation of Spectral Quantities	32
3.3.2 Overlapped Windowing	33
3.3.3 Composite Windowing	34
3.3.4 Accuracy Metrics	35
3.4 Identification of the Model	37
3.4.1 Longitudinal Dynamics	38

3.4.2	Lateral Dynamics	42
3.5	Analysis and Discussion	46
4	Parametric Model Identification	48
4.1	Introduction	49
4.2	LOES Modeling	49
4.3	Rotorcraft Dynamics	50
4.3.1	Rigid-Body Model	52
4.3.2	Extension of the Rigid-Body Model	54
4.3.3	Model Linearization	55
4.3.4	LOES Model Structure	58
4.4	Parameter Estimation Methods	62
4.4.1	Maximum Likelihood Estimator	63
4.4.2	Output-Error Method	64
4.4.3	Frequency-Response-Error Method	65
4.5	Nonlinear Estimation Routines	67
4.5.1	Levenberg-Marquardt Solution	67
4.5.2	Downhill Simplex Solution	71
4.6	Identification of the Model	74
4.6.1	Longitudinal Dynamics	75
4.6.2	Lateral Dynamics	77
4.7	Analysis and Discussion	79
5	Conclusion	83

LIST OF FIGURES

1.1	Schematic of system identification procedure	3
1.2	Schematic of the developed identification tool	7
2.1	Iterative procedure of input design	10
2.2	Conventional input types used in aircraft system identification	11
2.3	Example of two concatenated chirps applied on lateral stick of R-50 UAV helicopter for model identification in hover regime [1]	12
2.4	Examples of actual multi-step input: Excited lateral and longitudinal sticks of BO-105 helicopter used for hover model validation [2]	14
2.5	Schematic of the designed frequency sweep	20
2.6	Schematic of the designed doublet input	21
2.7	Trex-700 dimensions based on its operating manual	23
2.8	Armed Trex-700 used for identification experiment, © MicroPilot	24
2.9	Flight test results: measured input-output for longitudinal mode	27
2.10	Flight test results: measured input-output for lateral mode	27
3.1	Illustration of CZT in z-plane [3]	31
3.2	Measurement noise in input and output signals	33
3.3	Schematic of non-parametric SID tool	37
3.4	Estimated spectral functions for pitch motion	38
3.5	Estimated frequency-response function for pitch motion	39
3.6	Identification results for longitudinal mode	40
3.7	Accuracy metrics for longitudinal mode identification	41
3.8	Estimated spectral functions for roll motion	42
3.9	Estimated frequency-response function for roll motion	43
3.10	Identification results for lateral mode	44

3.11	Accuracy metrics for lateral mode identification	45
4.1	Swashplate mechanism of Align Trex-700, © MicroPilot	51
4.2	Rotor blades flapping motion [4]	52
4.3	Helicopter body-fixed frame [4]	54
4.4	Possible outcomes of a step in Simplex method (adopted from [5])	73
4.5	Schematic of the parametric SID tool	74
4.6	Identification results: OE method for short-period dynamics	76
4.7	Identification results: FE method for short-period dynamics	77
4.8	Identification results: FE method for roll dynamics	79
4.9	Identification results: OE method for roll dynamics	80

LIST OF TABLES

2.1	Different types of excitation input used in aircraft system identification	11
2.2	Key specifications of piloted sweep for system identification	13
2.3	Frequency sweep minor and major aspects	14
2.4	Major and minor aspects of multi-step input design strategies	16
2.5	Frequency range of interest for different applications	17
2.6	Frequency sweep design specifications	19
2.7	Examples of multi-step inputs employed in aircraft system identification	21
2.8	Doublet design specifications	22
4.1	LOES model structure for on-axis responses	62
4.2	Identification results: OE method for short-period dynamics	75
4.3	Identification results: FE method for short-period dynamics	76
4.4	Identification results: OE method for roll dynamics	78
4.5	Identification results: FE method for roll dynamics	78
4.6	Cramer-Rao bound for short-period dynamics	81

NOMENCLATURE

List of Symbols

f	Frequency, Hz
ω	Angular frequency, rad/s
f_s	Sampling frequency
T_{rec}	Record time
T_{win}	Window length
G_{uu}	Input autospectrum
G_{zz}	Output autospectrum
G_{uz}	Input-output cross-spectrum
ε_r	Random error estimate
γ^2	Coherence function
$\tilde{H} \hat{H} \hat{H}_c$	Rough, smooth, and composite frequency-response estimates

$u \ v \ w$	Translational velocities
$p \ q \ r$	Angular rates
$\phi \ \theta \ \psi$	Euler angles
$X \ Y \ Z$	Aerodynamic forces
$L \ M \ N$	Aerodynamic moments
$\delta_{lon} \ \delta_{lat} \ \delta_{col} \ \delta_{ped}$	Control inputs
$I_{xx} \ I_{yy} \ I_{zz}$	Moments of inertia

J	Cost function
θ	Vector of unknown parameters
M	Hessian matrix
S	Sensitivity matrix

\Re	Real part of a complex number
\dagger	Complex conjugate transpose

Abbreviations and Acronyms

UAV	Unmanned Aerial Vehicle
SID	System IDentification
SISO	Single Input/Single Output
MIMO	Multiple Input/Multiple Output
R/C	Radio-Controlled
PIC	Pilot In Control
IMU	Inertial Measurement Unit
DFT	Discrete Fourier Transform
FFT	Fast Fourier Transform
CZT	Chirp Z-Transform
PSD	Power Spectral Density
LOES	Low Order Equivalent System
DOF	Degree Of Freedom
OE	Output Error
FE	Frequency-response Error
CR	Cramer-Rao

Chapter 1

Introduction

Unmanned Aerial Vehicles (UAVs) are gaining more and more attention in recent years for their wide range of applications, specially their ever growing application in civil settings. The use of rotary-wing UAVs, compared to fixed-wing UAVs, is of higher demand due to their high maneuverability and fast control response. However, highly unstable flight dynamics, great degree of inter-axis coupling, and high sensitivity to control inputs, pose a great challenge in designing flight control systems for this type of UAVs, and additionally, make it difficult to find a mathematical model which can accurately and reliably capture their complex dynamics.

A major challenge in composing analytical model of an aircraft is to accurately characterize its aerodynamic behavior. The aerodynamic behavior of aircraft is characterized by a set of coefficients, known as aerodynamic derivatives, which describe the relationship between the aircraft motion variables and the aerodynamic forces and moments acting on the vehicle. The traditional method to evaluate the aerodynamic derivatives of an aircraft involves conducting the wind tunnel experiments on a scaled vehicle [6]. Despite effectiveness of the method, high expense of the experiments is the main barrier for the civilian UAV manufacturers to adopt it. In general, developing an accurate and consistent model for UAVs using conventional analytical

methods, where the contributions of structures, aerodynamics, and control systems can be seen explicitly, is difficult. This is mostly because of quick design cycles which does not allow enough time for developing such models during their production [7].

System identification has been examined and proved to be a reliable and less expensive alternative for analytical modeling of large-scale aircraft in the past [8]. However, for the case of unmanned aerial vehicles, more specifically unmanned helicopters, system identification has been utilized just in recent years [9]. System Identification (SID) is basically a process that provides a model that best characterizes the measured outputs to controls. In other words, identification techniques process time-domain measurements obtained from identification experiment for efficiently extracting accurate dynamic models of the system, whether parameterized or non-parametric. In non-parametric model identification, the frequency-response function of the system is estimated through time-frequency transformation and windowing techniques. For obtaining parameterized model, parametric identification is accomplished through sophisticated estimation and optimization algorithms which search the entire state space to extract aerodynamic coefficients that offer the best match between the actual data and the predicted data from the analytical model [10, 11].

The very first task in system identification is input design for flight test which must satisfy the persistent excitation conditions. The excitation inputs are designed to stimulate different modes of the aircraft and to provide rich information in output measurements. Another important task for identifying a realistic and reliable model is determination of model structure which requires some prior knowledge and insight about the system dynamics. Finally, designing and implementing the optimization algorithm is considered as the main challenge for an effective system identification. The concept of system identification is depicted schematically against analytical modeling in Figure 1.1.

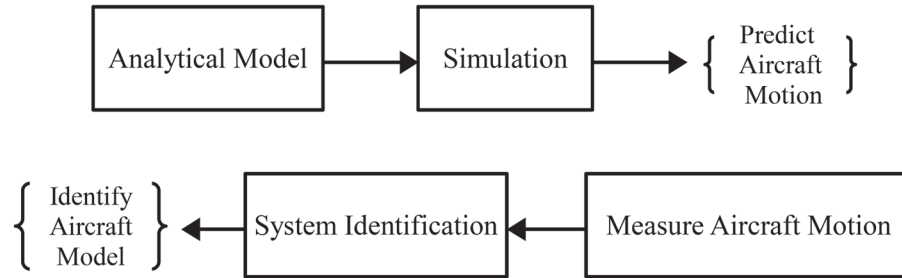


Figure 1.1: Schematic of system identification procedure

In general, system identification is classified into time-domain and frequency-domain methods. Due to numerous reasons, frequency-domain methods found to be particularly suitable to support the development of flight vehicle dynamics. Frequency-domain methods preliminarily calculate non-parametric model of the system without requiring a knowledge about the system dynamics, which provides an excellent insight into the key aspects of the aircraft behavior and can be utilized in parametric model identification. Besides, frequency-based methods are efficient in computations, since the calculations are algebraic and do not involve integration or differentiation, the number of data points to be processed are much less than time-domain methods, and the bias effects of noise in measurements and process noise are eliminated so there is no need to identify the error due to noise. Moreover, frequency-domain methods provide direct and independent measures for data quality and identification accuracy. They are also capable of performing model fitting in a specified frequency range. Time-domain methods, on the other hand, give more accurate and optimistic estimates, are time-optimal in terms of excitation inputs which involves shorter record length, and are well suited for nonlinear identification techniques. Time- and frequency-domain methods are similar in a sense that they both require satisfactory excitation to give a reasonable accuracy. Also, both methods deliver parametric models in form of state-space and transfer function representation [12].

There are few software tool developed for performing system identification for aerial vehicle applications [8]. The best example is the Comprehensive Identification from FrEQUENCY Responses (CIFER) system identification facility which has been developed by NASA Ames Research Center. CIFER is an integrated set of system identification programs and utilities which supports frequency-domain identification techniques for estimating non-parametric, transfer function, and state-space models from a given dataset. CIFER, as a user-specified tool, is considered to be one of the top resources for frequency analysis, and a reliable system identification tool [12]. Another identification tool which has been used successfully for aerial vehicle applications is the System IDentification Programs for AirCraft (SIDPAC) developed at NASA Langley Research Center. SIDPAC is a consistent identification facility which offers a variety of identification techniques and utilities in time- and frequency-domain [13].

Original attempts for modeling small-scale helicopters using system identification trace back to a study by Mettler in 1999 [1] in which model identification methods for full-scale helicopters were adopted for smaller aerial vehicles using dynamic scaling techniques. Later, in some relevant works, Mettler employed different identification methods to predict reliable hover and cruise models for Yamaha R-50 and X-Cell unmanned helicopters, with applications to flight control design and simulation [9, 14–16]. These works proved that system identification from flight data work quite well for smaller unmanned helicopters provided that a proper model structure has been developed in the first place [16].

To our knowledge, various identification methods have been used in order to predict dynamic models for different types of small or miniature scale helicopters up to now. Most of the works are concentrated on frequency-domain and linear identification methods, and exploited CIFER as the SID tool. A state-space model is identified for *Nusix* Radio-Controlled (R/C) helicopter in hover condition using

Matlab System Identification Toolbox [17]. A comprehensive parametric model for *Honeybee* miniature helicopter in hover regime is predicted using CIFER and SID-PAC techniques [18, 19]. Yuan et al introduced a novel two-stage method for hover model identification of *Hirobo Eagle* helicopter, in which high quality initial values for parameters are determined through a pre-estimation process [20]. Chowdhary et al examined a recursive identification method which utilizes different types of Kalman filter for both state and parameter estimation of *Artis* unmanned helicopter in hover regime [11]. Finally, a parametric state-space model for heave dynamics of *Samara* miniature rotorcraft, with application to controller design, is determined from flight test data [21].

Fewer researches have focused on transfer function identification of small-scale helicopters, compared to state-space modeling techniques. Theodore et al developed a rapid frequency-domain modeling method for UAV flight control applications [7]. Dominant dynamic modes of *Ikarus* miniature helicopter are characterized using a novel transfer function identification technique introduced by Kim et al [22]. Al-Radaideh et al compared usage of CIFER and Matlab for predicting a transfer function model to capture attitude dynamics of *Joker3* helicopter [23]. Cai et al identified a low order transfer function model for augmented yaw dynamics of *Helion* UAV helicopter using CIFER, based on which a flight control system for yaw channel is designed [24].

1.1 Research Motivation

Simulation results of our computer simulation software exhibit discrepancy with respect to the actual data from the flight tests of our rotary-wing UAV test-beds. A significant portion of such dissimilarity is attributed to inaccuracies associated with the aircraft analytical model within the simulation software. This reduces reliability

level of any control design conducted based on the simulation software, and in turn increases the need for further investigation, validation and tuning through the flight tests which is expensive and time consuming. One solution to this problem is employing identification methods. Hence, the motivation of this work is to develop SID tool for rotary-wing UAVs based on flight test measurements for the purpose of establishing more realistic and accurate simulation models, optimum system analysis, and more efficient controller design.

The SID tool is designed to be embedded in the computer simulation software available for the UAV platforms. This will help improving the reliability of simulation by providing more accurate models for the aircraft, compared to analytical models obtained from first principles. It is also considered as a preliminary stage in developing a framework for online or in-flight system identification with applications to fault-tolerant and adaptive control law design. Furthermore, the identified transfer functions can be used in the control system design process to reduce number of flight tests required for fine tuning the controllers on our UAV platforms.

The system identification tool, which is composed based on Matlab, gets the input-output measurements, performs a data post-processing, and gives the best non-parametric and parametric models of the system. This tool utilizes frequency-domain Single Input/Single Output (SISO) identification techniques, namely frequency-response and transfer function modeling, however with minimal modifications, it is extendable for Multiple Input/Multiple Output (MIMO) state-space identification. In order to verify its reliability, we tested the developed tool with real flight data, and compared the results with CIPHER, as a highly reliable tool in aircraft system identification. The aircraft used for identification experiment is a Trex-700 commercially available R/C helicopter designed by Align Corporation. The flight experiment is conducted in hover regime for dominant dynamic modes, namely pitch and roll motions, by MicroPilot Inc. The flowchart of Fig. 1.2 illustrates the logic behind our SID tool.

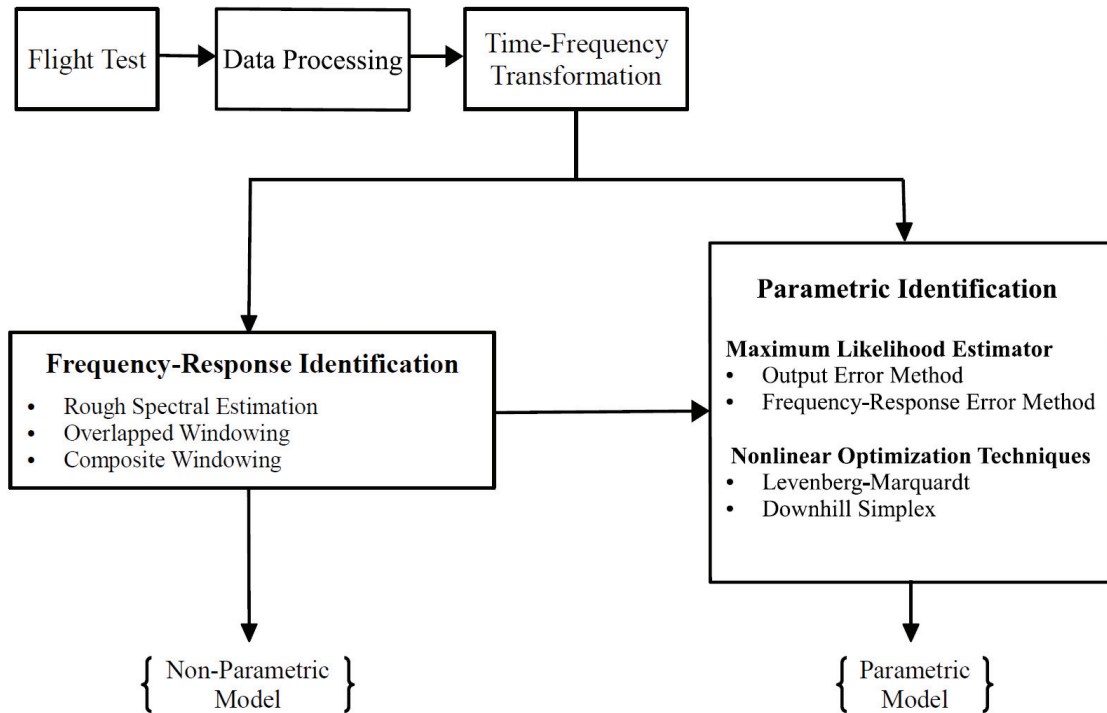


Figure 1.2: Schematic of the developed identification tool

1.2 Thesis Outline

The outline of the thesis is as follows. Chapter 1 gives an introduction to the concept of UAV system identification, reviews the recent literature, and describes the motivation of this research. Chapter 2 covers our study on flight experiment design, introduces our test-bed, and presents the flight test measurements. Chapter 3 deals with theory, implementation, and results of frequency-response identification from the measured data. Chapter 4 begins with our study about small-scale helicopter flight dynamics and model structure determination. This chapter also explains estimation and optimization techniques we have employed for parametric identification of our target vehicle, and presents the identified transfer function models. Chapter 5 draws the conclusion and outlines the future extensions of this study.

Chapter 2

Flight Experiment

From a technical point of view, this chapter summarizes flight experiment design for model identification of a small-scale helicopter. Two types of excitation inputs are designed, namely frequency sweep and doublet, in order to excite dominant attitude dynamics of the flight vehicle. The frequency sweep excitation will be used for model identification, and the doublet excitation will be employed in later flight tests for model validation. Specifications of each input are summarized, and their minor and major aspects are discussed. Moreover, our test-bed is introduced, and the key practical considerations for conducting the identification flight test are elaborated. Finally, the flight test results are presented, and the post-processing operations used for conditioning the data is explained.

2.1 Introduction

Rotorcraft system identification is quite dependent upon acquired flight data as an essential component of the identification. The richer the data, the more accurate and reliable model can be identified. Hence, within all possible flight inputs which can be used to excite the aircraft and collect the response data, those should be chosen and designed that provide richer information about the system.

R/C helicopters, because of their high maneuverability, agility, and smaller scale, have a quite different dynamic compared to large-scale or manned helicopters. This certainly affects the way the system should be excited in a general flight maneuver, or in an identification flight test. Different types of flight input have been examined and proved to be reliable in the past for the purpose of system identification of large-scale aircraft; however, for the case of unmanned aerial vehicle, and more specifically model scale helicopters, the literature does not offer a single or an optimum solution. Therefore, designing the flight input, in an optimum manner, is desirable and is of very high importance.

In general, the experiment design is conducted in an iterative procedure, through which an initial design is refined using the information obtained from non-parametric identification and model analysis. In other words, within the input design procedure, a non-parametric model will be identified, in order to check how good the aircraft has been excited. Based on a simple model analysis, the input design parameters will be refined and the values are updated. This procedure is repeated until the design parameters converge to an optimum value in a practical sense [25]. A schematic of the input design procedure is shown in Fig. 2.1. This work focuses on the initial stage of input design. In this stage, firstly, different types of identification inputs are reviewed. Then, based on our identification requirements, theoretical design rules, practical constrains, and pilot opinion, a detailed design for excitation inputs is accomplished. Furthermore, an operational plan is outlined for flight test implementation. The results of the initial input design will be used in order to conduct flight experiment and collect measurement data.

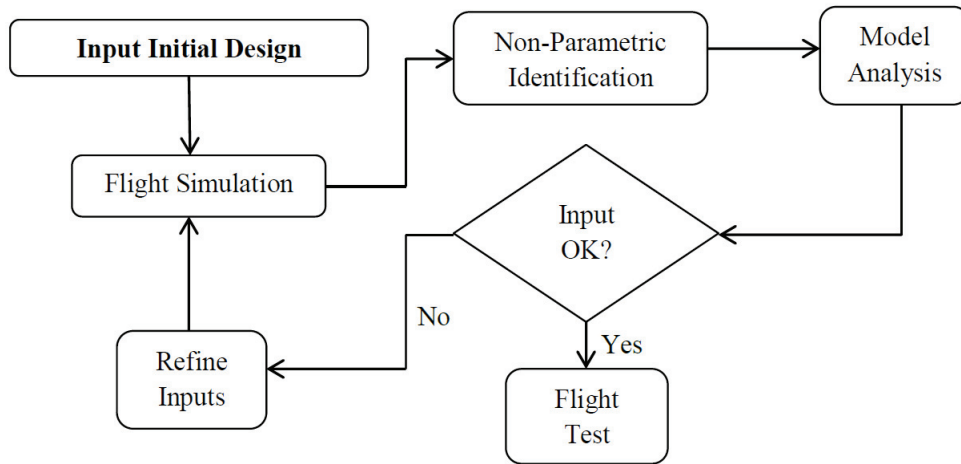


Figure 2.1: Iterative procedure of input design

2.2 Scope of Input Design

For system identification of fixed-wing and rotary-wing flight vehicles, input excitation can be categorized under two classes, heuristic and non-heuristic inputs [26]. Heuristic inputs are those applied mostly in frequency-domain identification methods, which have been widely used in rotorcraft model identification, and do not require a priori knowledge of system dynamics. Piloted (or automated) frequency sweep, impulse, and multi-sine (such as Shroeder-Phase, Mehra, and DUT) inputs are classified as heuristic inputs. In contrary, designing non-heuristic inputs requires some prior knowledge of dynamic behavior of the system. In addition to optimal inputs, conventional multi-step inputs (such as doublet, 3211, 211, etc.) are categorized as non-heuristic inputs. These inputs are commonly used in time-domain identification methods, as well as model verification [27]. Table 2.1 summarizes identification input types. A schematic of different identification inputs is illustrated in Fig. 2.2.

In order to design a proper input signal, we have to recognize input parameters

first. Input shape or type is considered as the first variable in the design procedure which is chosen in initial design step and is kept fixed during the design loop. Frequency range, amplitude envelope, and maneuver time are the variables to be adjusted during the iterative design procedure of the input after they have been assigned a primary value in the initial design phase.

Table 2.1: Different types of excitation input used in aircraft system identification

Input Class	Type	Subcategory		
Heuristic	Impulse	One-sided		Two-sided
	Frequency Sweep	Piloted		Automated
	Multi-Sine	Shroeder-Phase	Mehra	DUT
Non-Heuristic	Multi-Step	Doublet	3211	211
	Optimal Inputs	Estimation Error		Engineering Approach

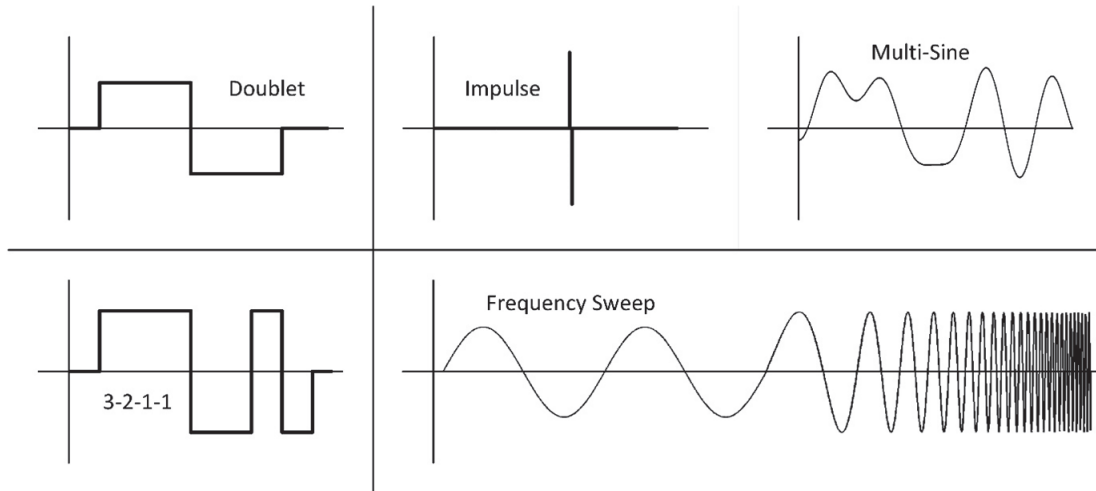


Figure 2.2: Conventional input types used in aircraft system identification

In order to choose a proper input shape, two basic considerations have to be taken into account: excitation capability of the desired dynamic mode and pilot implementation constraints. Hence, for choosing an input type among all conventional and optimal options, specification of the different inputs should be known first,

then a comparison has to be made, and finally the types that are in agreement with identification requirements, which are capable of maximum excitation, and can be practically applied by pilot, should be selected. By studying various identification inputs, two types have been chosen. Piloted frequency sweep as well as doublet multi-step input for model identification and verification, respectively. In the following sections, specifications of these inputs are discussed. Also, the main reasons for selecting these inputs are elaborated.

Frequency Sweep

Frequency sweep or frequency chirp is a class of control inputs having a quasi-sinusoidal roughly symmetric shape with a positive frequency progression. Frequency sweeps are considered as heuristic excitation as no prior knowledge of the system dynamics is required for them in design and implementation. Besides, frequency sweeps have a very uniform distribution of spectral content which can guarantee persistent excitation, and result in accurate frequency-response identification. A typical frequency sweep for aircraft system identification generally starts from a trim condition, continues with two cycles of lowest defined frequency, progresses with smoothly increasing frequency pattern, reaches a predetermined high frequency, and finally gets back to the trim condition from which it started [12] (see Fig. 2.3).

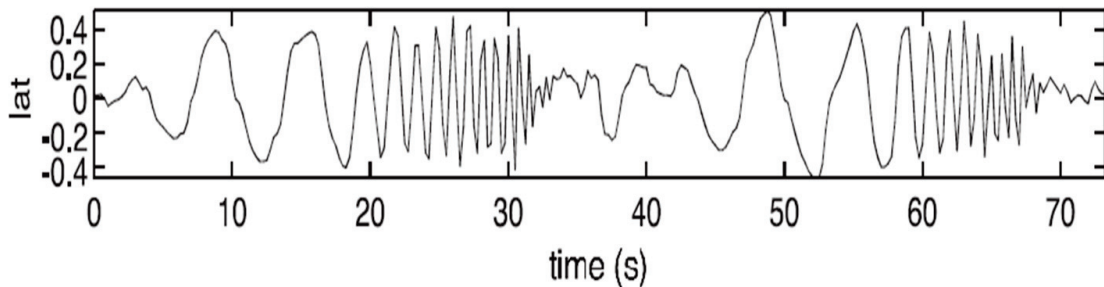


Figure 2.3: Example of two concatenated chirps applied on lateral stick of R-50 UAV helicopter for model identification in hover regime [1]

Having roughly symmetric time-history responses is a beneficial aspect of frequency sweeps. It helps to maintain the aircraft centered around trim condition and is important in determination of trim value in spectral analysis. In addition, frequency sweep is a safe input from operational aspect as minimum and maximum frequencies are predetermined which prevents overstressing aircraft modes such as lightly damped structural modes. Key features for implementation of a piloted frequency sweep are summarized in Table 2.2.

Table 2.2: Key specifications of piloted sweep for system identification

What is important	What is NOT important
Start and end in trim	Constant amplitude
Two complete long-period inputs	Exact sinusoidal shape
Smooth increasing frequency progression	Exact frequency progression
Rough symmetry about trim	Exact repeatability
Non-swept inputs for off-axis channels	Higher amplitude in high frequencies

However using frequency sweep can guarantee persistent and accurate identification results without having a priori knowledge of system, there are some minor aspects regarding this class of input that should be considered. Having a wide bandwidth can help enriching response information content; although, it can be critical in minimum and maximum frequencies. In other words, it is hard to maintain flight condition in low frequencies, and in higher frequencies, lightly damped structural modes, or some aircraft system modes could be excited unintentionally. Besides, for MIMO systems, using frequency sweep is not practical, so their usage is limited to SISO systems. Moreover, frequency sweep requires considerably longer record time compared to other identification inputs. Hence, using frequency chirp for cases in which a short flight time is necessary (e.g. high-angle-of-attack aircraft) is not feasible [12]. In Table 2.3, major and minor aspects for frequency sweeps are listed.

Table 2.3: Frequency sweep minor and major aspects

Major Aspects	Minor Aspects
Easy pilot implementation	Not suited for MIMO systems
Prior knowledge is not required	Not optimum SID results
Persistent and reliable SID results	Unintentional high frequencies excitation
Accurate SID results	Hard to keep flight condition in low ω
Large bandwidth	Long duration record time

Multi-Step input

Multi-step inputs are a combination of simple step pulses with different pulse width in positive and reverse directions. In a pulse signal, which is the simplest way to excite the oscillatory motion of aircraft, the control input is active for a certain amount of time, then released for the aircraft to freely respond about its trim condition. Doublets, 3211, 1123, 211 are different types of multi-step signals used in system identification. Herein, the specification of doublet and 3211 multi-step inputs are discussed as popular inputs in aircraft model identification and validation.

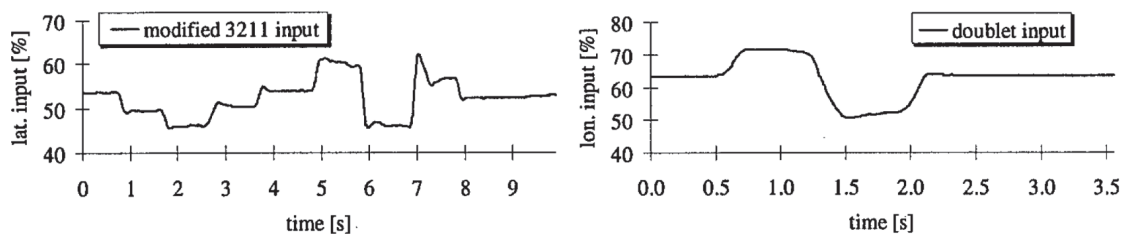


Figure 2.4: Examples of actual multi-step input: Excited lateral and longitudinal sticks of BO-105 helicopter used for hover model validation [2]

Doublet input is a symmetrical two-sided pulse in which the control stick is moved abruptly from trim position and held fixed for a predetermined time step Δt . Then, in a symmetric fashion, the control is moved abruptly again in the reverse

direction and held fixed for the same amount of time, and finally, released quickly to get back to its initial trim value. The 3211 multi-step input is similar to doublet from two aspects: the sudden control reversal and the trim start and end points. However, 3211 input composed of four linked pulses the width of which is varying in a decreasing manner, i.e. $3\Delta t$ for the first pulse, $2\Delta t$ for the reversed pulse, and two $1\Delta t$ for the doublet shape pulse at the end. Figure 2.4 depicts actual 3211 and doublet inputs applied to helicopter system identification [25].

Doublet can be considered as square wave approximation of sine wave having a broader bandwidth. However, its energy is more concentrated on the frequency of the corresponding sine wave characterized by Δt . In designing doublet and 3211, time step Δt is chosen based on the Eigen frequency of desired flight mode to be excited which is known a priori. That is why these inputs are classified as non-heuristic inputs. Time variations and multiple step reversals in 3211 input provide a much broader bandwidth compared to the doublet input. Higher band width allows for 3211 to adequately excite a band around natural frequency of the flight mode of interest; however, doublet is more flight condition dependent. The 3211 input is also called *poor man's frequency sweep* for its similarity to frequency sweep in covering a wide range of frequencies [28].

In helicopter system identification, doublet is generally used for model verification, mainly because it is different enough from frequency sweep as a common input for helicopter identification. This is good to assure that the identified model is not dependent on a specific type of input. Doublets are also proved to be well suited as directional input (rudder/pedal) in identification. Likewise, it has been proved that 3211 is more suitable as longitudinal input (elevator/cyclic pitch). Both doublet and 3211 are easier in execution than frequency sweep. Also, similar to frequency sweep, in doublet and 3211, duration and exact shape is of second importance [12]. Compared to doublet, 3211 is an asymmetrical input ($4\Delta t$ positive pulse and $3\Delta t$ negative

pulse), which will affect the spectral analysis in finding the spectral estimate of trim values. Similar to frequency sweep, larger duration of initial pulses in 3211 can cause the aircraft to deviate a lot from trim condition which is not desirable. These minor aspects of 3211 can be overcome using modified 3211, or using two linked 3211 with the second one having reversed polarity [28]. Minor and major aspects of doublet and 3211 are summarized in Table 2.4.

Table 2.4: Major and minor aspects of multi-step input design strategies

	Doublet	3211
Major Aspects	Easier pilot implementation than frequency sweep	
	Exact shape and pulse duration is of second importance	
	Suitable as directional input	Suitable as longitudinal input
	Suited for model verification	Suited for model identification
	Symmetric	Wide band input
Minor Aspects	A priori knowledge is required	
	Shorter band than 3211	Unstable response in low frequencies
	Flight condition dependent	Asymmetric

2.3 Input Detailed Design

The main input type chosen for the identification problem is frequency sweep for couple of reasons. Firstly, frequency sweep is recognized as a very reliable input in large-scale helicopter model identification. The use of frequency sweep in unmanned helicopter identification has been also examined in some works in the past resulting in persistent and reliable models [1]. Besides, as there is not enough information about the target helicopter, Trex-700, frequency sweep as a broadband input covering a wide frequency spectrum can be the optimum (not time-optimal) choice. Applying

frequency sweep requires a longer flight test, plus some consideration in execution by pilot, which is not an issue in this work. Consulting with the pilot, some ideas for implementation of the frequency sweep input are obtained, which are explained later in this thesis (see section 2.5). Besides, optimal inputs are omitted from our choice as they require an initial educated estimate of model parameters which is not available in our case. Likewise, it is better to avoid using doublet inputs for identification since doublets are more dependent on the flight mode being identified, and there is not sufficient information about the system available. However, doublet can be used for time-domain verification of the models identified using frequency sweep inputs, because it is different enough from frequency sweep in shape and pattern, and it is very simple and easy (easier than 3211 and frequency sweep) for pilot to apply.

2.3.1 Piloted Frequency Sweep

Design parameters of a piloted frequency sweep consist of frequency range of interest, amplitude range, and record time. For determining frequency range, it is desired to recognize minimum and maximum frequencies of interest to ensure acceptable accuracy of the identification over the range of applicability of the model. Table 2.5 shows frequency range of interest for different aerial vehicle applications [10, 12].

Table 2.5: Frequency range of interest for different applications

Application	ω_{min}	ω_{max}
Validation of simulation models	0.3	12
Flight control design	1	20
Typical pilot input	0.1	10
Handling quality specification	0.5	15

In the latter row of Table 2.5, minimum and maximum frequencies are related to bandwidth frequency ω_{BW} and -180 -deg phase frequency ω_{180} in a way

that $\omega_{min} = 0.5 \omega_{BW}$ and $\omega_{max} = 2.5 \omega_{180}$, both of which can be determined from frequency-response function of the system. As an example, ω_{BW} and ω_{180} for bare airframe of a helicopter have typical values of 1 and 6 rad/s respectively [12]. In selection of frequency range for the input, the domain of application in addition to feasibility of execution by pilot should be considered. For example, for validation of simulation models, lower frequencies are of high importance; however, for flight control design application high end frequency is more important. According to the identification requirements, following the general guidelines stated in Table 2.5, and having considered that the pilot is capable of applying inputs up to the frequency of 2 Hz (≈ 12.5 rad/s), the frequency range is selected as follows. These values are selected as an initial guess and will be fine-tuned in the iterative procedure for later flight tests.

$$0.3 \leq \omega \leq 12 \text{ rad/s} \quad (2.1)$$

According to a general guideline [12], frequency sweep record time has to be equal or greater than a certain value proportional to maximum period of excitation as $T_{rec} \geq 4.5T_{max}$. Considering the initial value for minimum frequency (maximum period), the record time is obtained as $T_{rec} = 90$ s. As mentioned previously, a piloted frequency sweep used for identification purpose requires to start in trim condition, follows with two cycles of minimum frequency (0.3 rad/s in our case), covers the frequencies between ω_{min} and ω_{max} smoothly, and finally, ends also in trim condition. For both start and end of the input signal, 3 seconds of trim input is considered with two initial low frequency cycles having the period of 20 seconds.

The amplitude of identification input should be strong enough at each time step to be able to excite the dynamic mode of interest, i.e. it should be greater than a minimum value. Besides, it cannot be greater than a certain value because it might corrupt the linearity assumptions of the model. Following a general rule of thumb [12], the control input has to be within the range of $\pm 10 - 20\%$ of input

full range. From the aircraft response point of view, these lower and upper limits for attitude angles should be $\pm 5 - 15$ deg. In a same manner, angular rates should lie within the range of $\pm 5 - 15$ deg/s, and forward velocity should not exceed the limits of $\pm 5 - 10$ kn. The response of aircraft has to be kept within this predefined envelope and inputs which might cause the response to exceed these ranges should be avoided. This can be done with the help of data telemetry during flight test. It is also recommended that signal amplitude starts and ends with a gradual phase-in and phase-out respectively [12]. The results of the frequency sweep detailed design are summarized in Table 2.6. Figure 2.5 illustrates a schematic of the designed frequency sweep.

Table 2.6: Frequency sweep design specifications

Design Parameter	Value	Units
Frequency range	0.3 - 15	rad/s
Record time	90	s
Period of initial/final trim	3	s
Amplitude envelope	$\pm 10 - 20$	%
Attitude response limitations	$\pm 10 - 15$	deg
Angular rate limitations	$\pm 10 - 15$	deg/s
Forward velocity limitations	$\pm 5 - 10$	kn

2.3.2 Doublet Input

In designing the doublet input, the parameter to be selected is the time step of the signal. Optimum range of frequencies of multi-steps is a range below and above the natural frequency of the mode being excited. This frequency range is characterized by the shape, duration, and time step of the multi-step. Based on a design rule of

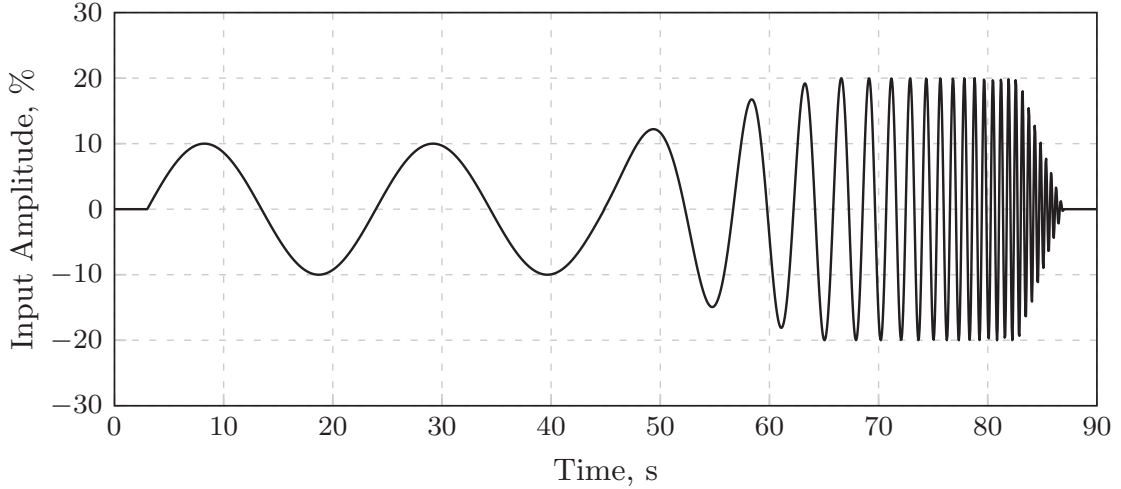


Figure 2.5: Schematic of the designed frequency sweep

thumb [28], the time step for the doublet is given in terms of natural frequency of the desired mode in equation (2.2).

$$\Delta t_{dbl} = 0.5 T_{osc} = 3.142/\omega_n \quad (2.2)$$

By knowing the period of oscillations of the flight mode a priori (T_{osc}), the time step of the doublet input for exciting that mode can be determined. In our design, we decided on an initial educated guess for the time step by studying multi-steps used for identification of various rotary-wing and fixed-wing aircraft. In order to find an initial guess for the time steps, multi-steps used for identification of Yamaha R-50 are considered [9]. In that research, a combination of doublets and 3211 inputs are used for identification of different modes of R-50 helicopter in hover and cruise flight regimes. The time step of 3211 used for collective pitch stick is about 0.5 sec. The time step of the doublets (Δt_{dbl}) applied to cyclic inputs as well as directional input varies between 1 to 2 seconds. Moreover, in LOES identification of Tu-144LL fixed-wing aircraft [29], a 211 type of multi-step is used for longitudinal stick with the time step of about 1.5 seconds. In another application for identification of the DLR BO-105 helicopter [2], doublets applied as cyclic input have the time step of

about 1.5 seconds, and 3211 has the time step of approximately 1 second. Finally, a series of linked doublets is used as the elevator input for identification of F-18 High Alpha Research Vehicle [30] with the time step of roughly 0.75 s. A summary of these information are collected in Table 2.7.

Table 2.7: Examples of multi-step inputs employed in aircraft system identification

Aircraft	Input Type	Δt sec
Yamaha R-50 UAV Helicopter	doublet	1-2
	3211	0.5
DLR BO-105 Helicopter	doublet	1.5
	3211	1
Tu-144LL Supersonic Aircraft	211	1.5
F-18 High Alpha Research Vehicle	linked doublets	0.75

Finally, two linked doublets with reversed polarity are considered with a time step adopted from similar aircraft data. Amplitude ranges will be the same as the frequency sweep, i.e. $\pm 10 - 20\%$ of the input full range. The results of the initial design are summarized in Table 2.8. Figure 2.6 illustrates a schematic of the designed doublet input.

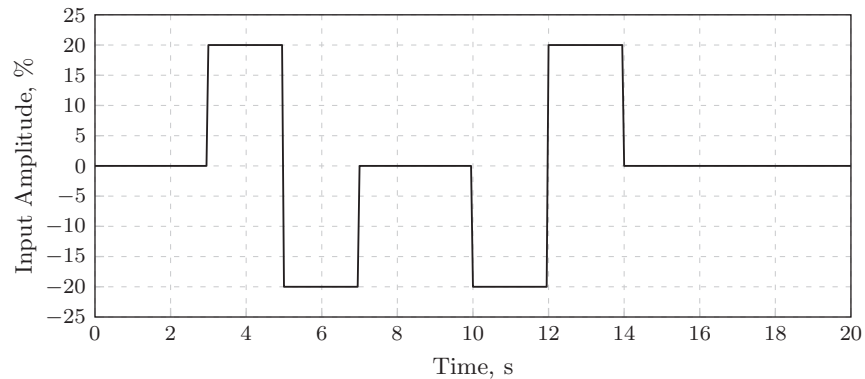


Figure 2.6: Schematic of the designed doublet input

Table 2.8: Doublet design specifications

Design Parameter	Value	Units
Time step	2	s
Record time	20	s
Period of initial trim	3	s
Period of final trim	6	s
Amplitude envelope	$\pm 10 - 20$	%
Attitude response limitations	$\pm 10 - 15$	deg
Angular rate limitations	$\pm 10 - 15$	deg/s
Forward velocity limitations	$\pm 5 - 10$	kn

2.4 Introduction to the UAV Testbed

For flight test purpose of this research work, we have used a Trex-700 airframe equipped with MP2128G2Heli MicroPilot autopilot. Trex-700 is a commercially available unmanned helicopter designed by Align Corporation using a flybarless rotor system, having approximate gross weight of 4200 g, main rotor diameter of 1602 mm, and tail rotor diameter of 281 mm, and utilizing a brushless electric motor, and a collective-pitch rotor configuration [31]. Major dimensions of the vehicle are illustrated in Fig. 2.7.

The autopilot is armed with 3 MEMS gyros to measure the angular rates of the vehicle in the body-fixed frame. It is also equipped with 3 accelerometers to measure translational accelerations, and a GPS and a Compass for navigation purpose. The autopilot utilizes a Kalman filter to estimate the unknown and unmeasured states, in order to compensate for the inaccuracies in the sensor measurements. Hence, the angular rates as the output measurement extracted from the autopilot are not direct sensor outputs, but corrected for bias error and sensor drift through an onboard

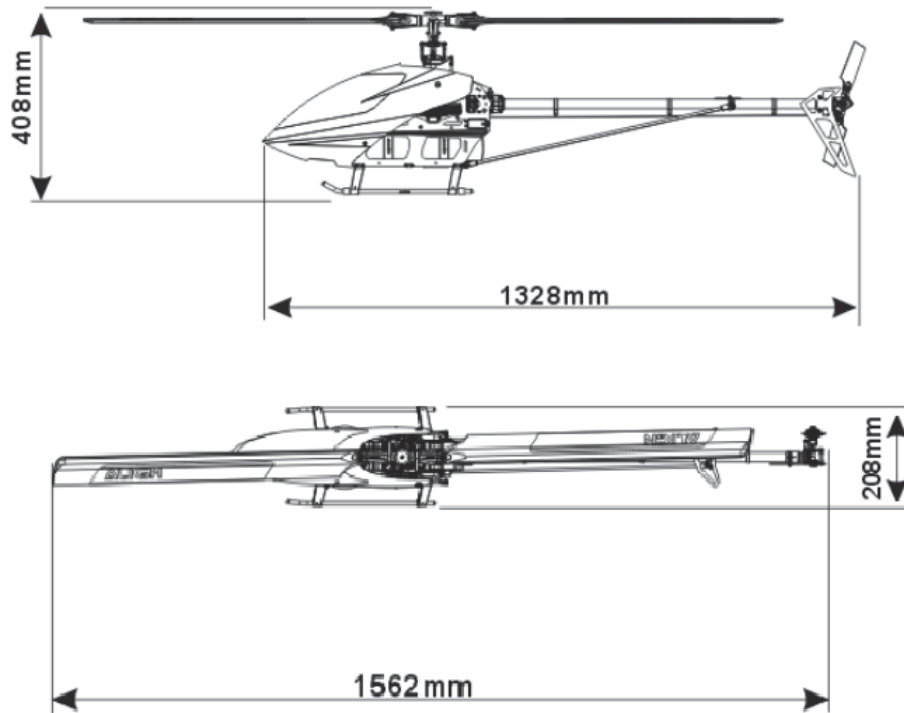


Figure 2.7: Trex-700 dimensions based on its operating manual

algorithm. The autopilot also utilizes a yaw-rate feedback system to augment the stability of yaw dynamics. Except for the yaw mode, which requires a mandatory control system, a Pilot-In-Control (PIC) flight test is performed for identification experiment. The pilot cyclic and collective commands as input measurements are measured through an onboard radio receiver system. The autopilot is located almost at the center of gravity of the vehicle, and the data are logged at sampling frequency of 30 Hz. Figure 2.8 depicts the flight-test vehicle equipped with MP2128G2Heli autopilot.

2.5 Flight Test Implementation

The flight test for the purpose of system identification are fundamentally different from general flight maneuvers for which pilots are trained. Pilots tend to control



Figure 2.8: Armed Trex-700 used for identification experiment, © MicroPilot

the aircraft based on its response due to controls, however for identification flight experiments pilot is not allowed to correct for controls based on the aircraft reaction. There are some practical notes that must be taken into account by pilot when performing the flight experiment so that a higher quality flight data can be acquired. Here, the points that have a key role in system identification flight test, adopted from references [4, 12], are discussed. An experienced pilot has conducted the identification flight test, and these practical techniques are tried to be employed in execution of the flight test.

What Is Not Important: It is not necessary to keep a constant amplitude, exact sinusoidal shape, and exact frequency progression during a sweep excitation. In fact, some irregularities in shape, frequency and amplitude are desired in order to enrich the sweep input. In addition, as the sweep reaches higher frequencies, it is not required to increase its amplitude in order to compensate the naturally diminished rate-response. For the concatenated sweep maneuvers, exact repeatability of input, again, is not important, as some roughness can augment the information content of the recorded data. This is also the case for the doublet input.

What Is Important: Some irregularity in the piloted inputs are appreciated, however, there are some factors that are important and must be noted. Starting from and finishing in the trim condition, emphasizing the higher periods (lower frequencies) in first half of the record time, having a smooth frequency progression without rushing to higher frequencies, and not exceeding the high end frequency are highly important in sweep excitation. The same rules apply for doublet excitation.

Off-Axis Excitation: While the pilot is applying a sweep/doublet to one control and monitoring the corresponding on-axis response, all other controls should be kept roughly symmetrical to the reference flight condition in order to bound the off-axis responses. For example, if the mode being excited is the short-period pitch mode by applying a sweep to longitudinal cyclic control, it is desired to keep lateral cyclic, collective and pedal controls symmetric with lowest possible amplitude to maintain the off-axis responses within a reasonable range. In other words, pilot should be advised to concentrate on the primary input, not to correlate the on-axis responses with the secondary controls.

Task of the Copilot: Pilot-applied sweeps and doublets are best done when two crews are involved, one in charge of the input and the other calling the tune. The copilot should provide the timing indicators to assist the pilot in conducting the flight test. The copilot can call out the time at certain times to signal the pilot when the control stick should be at a certain position. For the frequency sweep input, the pilot has to be signaled when the maximum frequency is approached and when it is reached. Telemetry data are also useful for monitoring the frequency progression in frequency sweep input.

Training, Practice, Safety: Experience has shown that pilots tend to increase the amplitude while the frequency increases. It is also difficult for a pilot to judge

about frequencies beyond 2Hz. It is recommended that the pilot practices while the vehicle is on the ground in order to realize the feel about the hand and feet motion required. Applying the inputs in a simulation environment is helpful as well. During the flight test, it is suggested that the pilot starts with simple sine waves with constant low amplitude, and then try to increase the frequency incrementally. It is necessary for the pilot to start the implementation of the designed inputs only when enough confidence has been gained to enhance the safety of flight test execution.

2.6 Flight Test Results

The flight test results used in this study belong to the excitation of pitch and roll on-axis responses only. Two frequency sweeps are applied to longitudinal and lateral cyclic inputs, denoted as δ_{lon} and δ_{lat} , respectively. The vehicle direct responses to these controls, namely pitch-rate q and roll-rate p , are measured accordingly. The measured data are passed through an anti-aliasing filter, and also corrected for effect of sensor drift. The post-processing procedure involves conditioning the data using a second-order low-pass filter with cut-off frequency of 25 rad/s, and removing the average value from all signals. Mean-removal operation will significantly increase the accuracy of identification in lower frequencies. Input-output data for longitudinal and lateral modes are illustrated in figures 2.9 and 2.10, respectively.

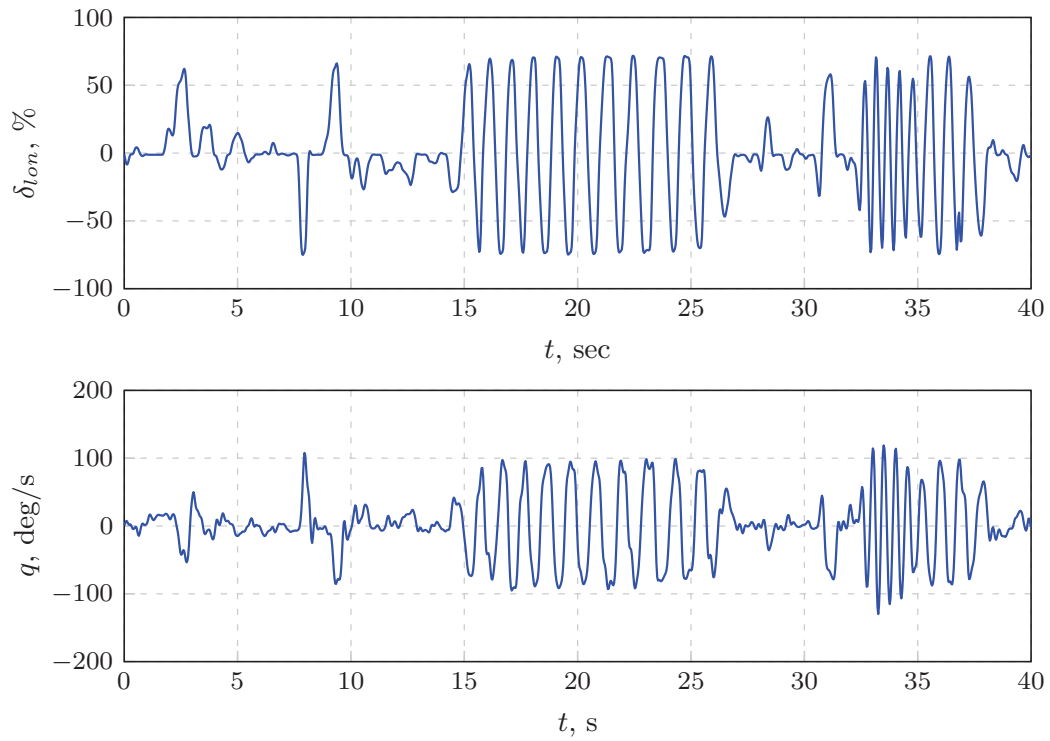


Figure 2.9: Flight test results: measured input-output for longitudinal mode

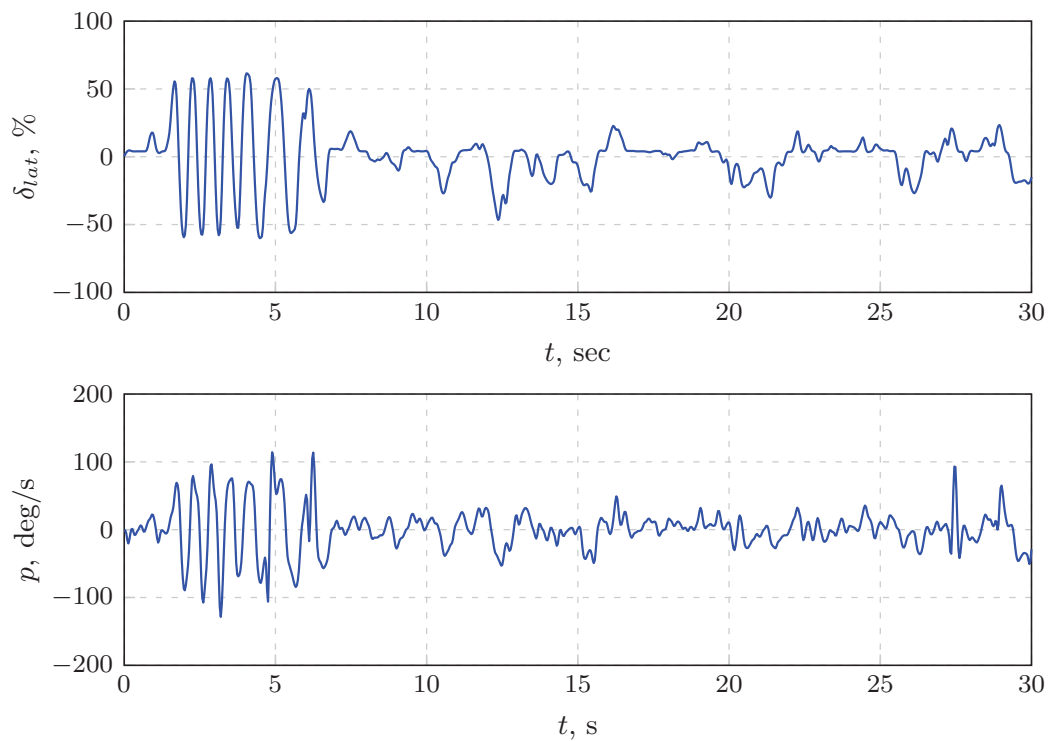


Figure 2.10: Flight test results: measured input-output for lateral mode

Chapter 3

Frequency-Response Identification

In the previous chapter, the flight-test vehicle was introduced, and the procedure for flight test execution and data collection is discussed. In this chapter, it is aimed to estimate an accurate and reliable non-parametric model for longitudinal and lateral dynamic modes of Trex-700 from the acquired flight data. This chapter begins with an introduction on frequency-response system identification issue. Sections 3.2 and 3.3 shed light on the theoretical aspects of the techniques used in the frequency-response identification. In Section 3.4, the identification results for Trex-700 helicopter obtained using a developed Matlab code are acquired. The results of the non-parametric models identified using CIFER toolbox are also given in this section. Finally, Section 3.5 concludes this chapter by providing an analysis for the identified models.

3.1 Introduction

Frequency-response system identification, also referred to as non-parametric model identification, is a modeling approach which attempts to estimate *frequency-response function* of a system from sampled input-output data. The frequency-response function is defined for any time-invariant system as the ratio of system output (response)

to system input (excitation) in frequency-domain. The term "frequency response" is essentially referred to the steady-state response of a linear time-invariant system when excited using a constant sine-wave input, which always results in a harmonic response with the same frequency of the excitation, a certain phase shift, and a magnified amplitude. This concept can be extended to a nonlinear time-invariant system if the fact that any arbitrary input signal can be expressed in terms of its periodic functions using Fourier series/transform is taken into account [32]. For a nonlinear system, the frequency-response function is the best linear model of input-output behavior which provides key information about the dynamic system characteristics. The advantage of this representation of system dynamics is that no prior knowledge and assumption for system structure or properties is required, except that the system is time-invariant [12].

The frequency-response system identification is widely used for dynamic system analysis, model validation for simulation, control system design, and more importantly, as a basis for parametric model identification [16] which is the main subject of Chapter 4. In following sections, we will introduce the methods that are used for finding an accurate estimate for the frequency-response function of a typical rotorcraft, as a nonlinear system, from measured input-output data.

3.2 Time-Frequency Transformation

Finding frequency-response function from a time-history dataset, firstly requires for the time-domain data to be transformed into the frequency-domain. The transformation methods commonly used in aircraft system identification are Discrete Fourier Transform (DFT), Fast Fourier Transform (FFT), and Chirp Z-Transform (CZT). The FFT is a quite faster method compared to the DFT, as it requires less data

points in calculations. However, the CZT is proved to be the most reliable and accurate method for frequency-response estimation which provides high flexibility in the selection of sample rates and frequency resolution [12].

The chirp z-transform of a sequence of N samples, x_n , can be interpreted as a general evaluation of z-transform over an arbitrary arc of the unit circle on z-plane of the form:

$$z_k = AW^{-k} \quad k = 0, 1, \dots, M-1 \quad (3.1)$$

where M is an arbitrary integer and A and W are as $A = e^{j2\pi\theta_0}$ and $W = e^{j2\pi\varphi_0}$. In the definition for A and W , the corresponding angles, θ_0 and φ_0 , are determined using the following equations:

$$\theta_0 = f_{min}/f_s \quad (3.2)$$

$$\varphi_0 = (f_{max} - f_{min})/f_s \quad (3.3)$$

where $[f_{min}, f_{max}]$ is the frequency range of interest, and f_s is the sampling rate of the sequence x_n . An illustration of these angles in z-plane can be found in Fig. 3.1. Having considered this, the chirp z-transform of a sequence of N samples x_n is determined from the following [3]:

$$X_k = \sum_{n=0}^{N-1} x_n (AW^{-k})^{-n}. \quad (3.4)$$

A special case of the z-transform in which a set of N points are distributed evenly around the entire unit circle in z-plane (rather than an arbitrary arc which is the case for CZT), is called Discrete Fourier Transform (DFT). Point's distribution and definition of the DFT can be determined as [12]:

$$z_k = e^{j2\pi k/N} \quad k = 0, 1, \dots, N-1 \quad (3.5)$$

$$X_k = \sum_{n=0}^{N-1} x_n e^{-jn k \frac{2\pi}{N}}. \quad (3.6)$$

The computation of the DFT requires N^2 complex multiplications and additions, however if N is a power of two, the computation will diminish to $N \log 2N$ operations.

This evaluation of the DFT, which is much more efficient in calculations, is called Fast Fourier Transform (FFT) [3]. A high accuracy evaluation of finite Fourier transform is used in SIDPAC for the time-frequency transformation [33]. Similar to CIFER, the chirp z-transform is employed as the transformation method in this study.

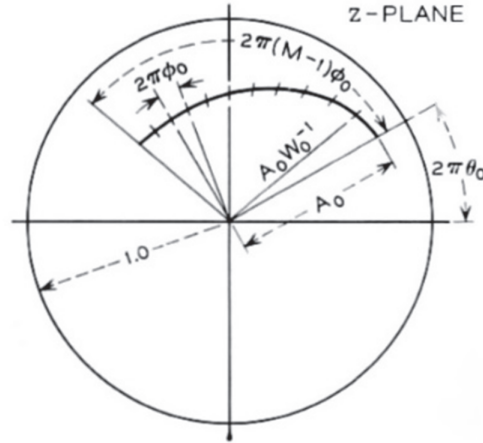


Figure 3.1: Illustration of CZT in z-plane [3]

3.3 Frequency-Response Function

In order to find the frequency-response function from the time-frequency transformation results, three methods are examined. Firstly, rough estimate of the frequency-response function $\tilde{H}(f)$ is obtained from rough spectral estimates. Secondly, smooth frequency-response estimate $\hat{H}(f)$ is determined from smooth spectral quantities using so-called overlapped windowing method. An improved estimation of the frequency-response function $\hat{H}_c(f)$ is obtained from taking a weighted average from several individual frequency-response functions each of which acquired from evaluating windowing method with a distinctive window length. The later method is called composite windowing which mixes the averaging benefits of smaller windows with dynamic range advantages of larger windows.

3.3.1 Rough Estimation of Spectral Quantities

The outcomes of time-frequency transformation of a typical input signal $u(t)$ and output signal $z(t)$, i.e. Fourier coefficients, $U(f)$ and $Z(f)$, introduce three important spectral functions. These spectral functions, which are rough estimates of input Power Spectral Density (PSD), output PSD, and input-output cross-spectrum (or cross-PSD), are determined from the following equations, respectively.

$$\tilde{G}_{uu}(f) = \frac{2}{T_{rec}} |U(f)| \quad (3.7)$$

$$\tilde{G}_{zz}(f) = \frac{2}{T_{rec}} |Z(f)| \quad (3.8)$$

$$\tilde{G}_{uz}(f) = \frac{2}{T_{rec}} [U^\dagger(f)Z(f)] \quad (3.9)$$

where $U(f)^\dagger$ denotes the complex conjugate of the input Fourier Coefficient $U(f)$ [34]. The PSD magnitude can also be displayed in power decibels as follows:

$$\tilde{G}_{uu_{dB}}(f) = 10 \log_{10}(\tilde{G}_{uu}(f)) \quad (3.10)$$

After the rough estimates of spectral densities are found, the frequency-response function $H(f)$ can be estimated from either one of the following expressions:

$$\tilde{H}_1(f) = \frac{\tilde{G}_{uz}(f)}{\tilde{G}_{uu}(f)} \quad (3.11)$$

$$\tilde{H}_2(f) = \frac{\tilde{G}_{zz}(f)}{\tilde{G}_{zu}(f)} \quad (3.12)$$

These expressions are considered as unbiased estimations of the frequency-response function provided that some assumptions about the measurement and process input/output noise are taken into account. They require some assumptions about the noises that might corrupted the time-domain signals. A general good assumption for $\tilde{H}_1(f)$ expression in aerial vehicle applications accounts for the output noise i.e. $\nu(t) \neq 0$, and neglects input measurement noise i.e. $u(t) \neq 0$. The input noise associated with unknown disturbances or unmeasured inputs, namely $p(t)$, are indirectly considered in the output noise $\nu(t)$ [12].

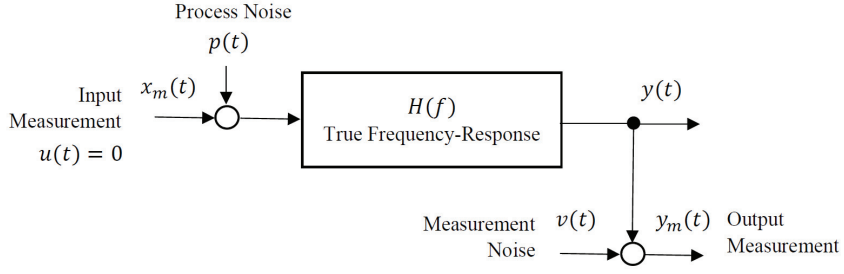


Figure 3.2: Measurement noise in input and output signals

3.3.2 Overlapped Windowing

In frequency-response estimation, one practical method which highly reduces the effects of random error in spectral estimates is called overlapped windowing or Periodogram. In this method, time-domain data is divided into shorter overlapping time segments or *windows* of length T_{win} . Each segment is then multiplied by a window tapering function $w(t)$ in order to reduce the error associated with side-lobe leakage in spectral estimates. Then, Fourier coefficients for each weighted time segment are determined separately. Finally, smooth estimate for the input signal, also referred to as input autospectrum denoted by $\hat{G}_{uu}(f)$, is obtained by averaging rough spectral estimate of each individual window as expressed in the following:

$$\hat{G}_{uu}(f) = (1/c_l n_r) \sum_{n=1}^{n_r} \tilde{G}_{uu,k}(f) \quad (3.13)$$

where n_r is the number of windows and c_l is the correction factor for the energy loss due to window tapering which depends upon the type of the window tapering function $w(t)$. The output autospectrum and cross-spectrum $\hat{G}_{zz}(f)$ and $\hat{G}_{uz}(f)$ are calculated similarly [12]. One tapering function that is commonly used in windowing techniques is Hanning function, which is also the tapering function employed in CIFER. A new research [35] shows that significant improvements in the results can

be achieved when a tapering function of the following form is used:

$$w(t) = \sin(\pi t/T_{win}) \quad (3.14)$$

which is referred to as half-sine function. Considering the aforementioned noise assumption, in addition to considering that the existing output noise is uncorrelated to input signal, one can determine the smooth frequency-response function from equation (3.5) by replacing rough spectral estimates with the smooth spectral estimates.

The challenge in the windowing technique is coming up with an optimum value for the window length T_{win} . Because, larger windows provide good frequency resolution in expense of reducing the number of averages which causes an increase in random error. While, shorter windows benefit from a lower random error in expense of limiting the dynamic range. As per guideline [12], a window length selected for time-domain data segmentation should be bounded in a range in which its lower and upper limits are given as:

$$\frac{T_{rec}}{2} \leq T_{win} \leq 20 \frac{2\pi}{\omega_{max}} \quad (3.15)$$

where ω_{max} is the maximum frequency of the excitation. In this study, an average value is chosen for window length, that is $T_{win} = (T_{rec}/2 + 40\pi/\omega_{max})/2$.

3.3.3 Composite Windowing

There is not an optimal single window length for estimating spectral quantities. The larger window provides higher frequency resolution with a more accurate identification in lower frequencies, while the smaller window increases the number of averages and reduces the random error accordingly in higher frequencies. Composite windowing technique is a solution to the challenge of window size selection.

In this method, the estimation for spectral quantities are improved by taking a weighted average of multiple spectral estimates each of which acquired from evaluating Periodogram method with a different value for the window length. In this

study, 5 window sizes are chosen with equal spacing from one another in order to cover the allowable range for T_{win} represented in equation (3.15).

In this approach, the smooth spectral quantities for each window size is calculated separately, e.g. $\tilde{G}_{uu,i}$ for input autospectrum, and i th window size. Then, they are combined in a weighted averaging manner in order to form a single accurate and reliable composite response. The weighting function for each window i and each frequency f is defined based on random error ε_r metric as follows (see section 3.3.4 for random error definition):

$$W_i = \left[\frac{(\varepsilon_r)_i}{(\varepsilon_r)_{min}} \right]^{-4} \quad (3.16)$$

where $(\varepsilon_r)_{min}$ is the minimum value for the random error of different windows length at a certain frequency point.

As an example, the input composite autospectrum at each discrete frequency is determined from:

$$\hat{G}_{uuc} = \frac{\sum_{i=1}^{n_w} W_i^2 \hat{G}_{uu,i}}{\sum_{i=1}^{n_w} W_i^2} \quad (3.17)$$

Having considered the aforementioned assumptions for input and output noise, the composite frequency-response function can be calculated from the composite spectral estimates as follows [12]:

$$\hat{H}_c(f) = \frac{\hat{G}_{uzc}(f)}{\hat{G}_{uuc}(f)}. \quad (3.18)$$

3.3.4 Accuracy Metrics

Two important products of the smooth frequency-response function are Coherence function and normalized random error. coherence function γ^2 , which gets a value between 0 and 1, is defined at each frequency point and determines how much the output spectrum is linearly attributable to the input spectrum. A mathematical

expression for coherence function is given in equation (3.19). The expected normalized random error in frequency-response magnitude and phase can be represented in terms of the estimated coherence function as shown in equation (3.20).

$$\gamma^2(f) = \frac{|\hat{G}_{uz}(f)|^2}{|\hat{G}_{uu}(f)||\hat{G}_{zz}(f)|} \quad (3.19)$$

$$\varepsilon_r(f) = C_\varepsilon \sqrt{\frac{(1-\gamma^2)}{2n_d\gamma^2}} \quad (3.20)$$

The parameter C_ε in equation (3.20) accounts for the window overlap, and n_d shows the number of independent time averages which is defined as $n_d = T_{rec}/T_{win}$ [34].

Similarly, for composite windowing method, coherence function and random error are determined from equations (3.19) and (3.20) by replacing the smooth estimates with the composite estimates. However, in random error equation, the window selection parameter n_d is calculated at each frequency based on the weighted-average window length at that frequency [12]:

$$\hat{T}_{win}(f) = \frac{\sum_{i=1}^{n_w} W_i^2 \hat{T}_{win_i}}{\sum_{i=1}^{n_w} W_i^2}. \quad (3.21)$$

In order to facilitate the comparison of two different identification methods or tools using the accuracy metrics such as coherence function and random error, *relative difference* of these metrics is computed. Equations (3.22) and (3.23) show the formulation of the relative difference between accuracy metrics calculated for two different identifications, the later for random errors, and the former for coherence functions.

$$\Delta\gamma^2 = \frac{\gamma_1^2 - \gamma_2^2}{\max\{\gamma_1^2, \gamma_2^2\}} \quad (3.22)$$

$$\Delta\varepsilon_r = \frac{\varepsilon_{r1} - \varepsilon_{r2}}{\min\{\varepsilon_{r1}, \varepsilon_{r2}\}} \quad (3.23)$$

The denominator of the relative difference formulation is supposed to get the better value (reference value), which corresponds to the higher accuracy in our case. Hence,

in equation (3.22), the difference between coherence functions is divided by the maximum coherence value. Also, in equation (3.23), the difference between random errors is divided by the minimum random error value. This is due to direct and inverse relations that coherence function and random error have with accuracy, respectively.

3.4 Identification of the Model

In order to find a nonparametric model for the flight vehicle, Trex-700, from flight test data, a Matlab code is developed. The processed input-output time-domain data for longitudinal and lateral modes are fed to the code. The program estimates the frequency-response function by employing three different methods presented in the previous section, i.e. rough estimation, overlapped windowing, and composite windowing. The program is quite capable of estimating a SISO non-parametric model for any set of input-output data, and it can be extended for MIMO identification. A schematic of the non-parametric SID tool is illustrated in Fig. 3.3.

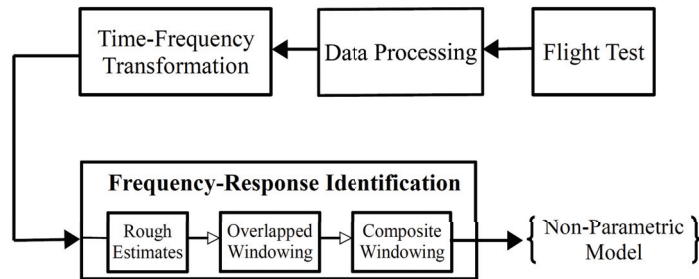


Figure 3.3: Schematic of non-parametric SID tool

The same set of data are fed to CIFER non-parametric identification packages (namely FRESPIID and COMPOSIT) to estimate a separate model for comparison. The results from CIFER and the developed Matlab code are presented in this section in the form of spectral functions, frequency-response function, and accuracy metrics. In order to assist the results comparison, relative difference between the accuracy

metrics obtained from CIPHER and the developed SID tool are given in this section.

3.4.1 Longitudinal Dynamics

The dataset used for the identification of longitudinal mode consists of longitudinal cyclic δ_{lon} as the input, and pitch-rate q as the output. The spectral functions, i.e. input, output, and cross-PSDs for longitudinal short-period mode are illustrated in Fig. 3.4. The results for frequency-response estimates from three aforementioned methods in form of Bode plot are depicted in Fig. 3.5, along with the corresponding accuracy metrics. Figure 3.6 shows the identification results obtained from the developed code and CIPHER. Figure 3.7 provides the accuracy measures to be used for validating each identified model, and comparing the results with one another.

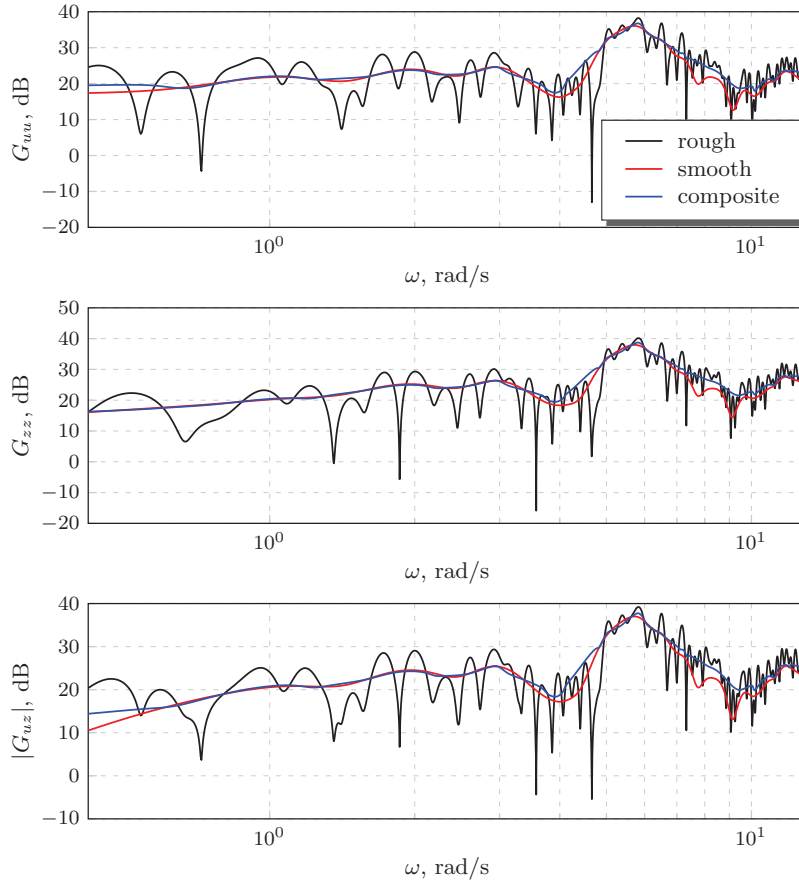


Figure 3.4: Estimated spectral functions for pitch motion

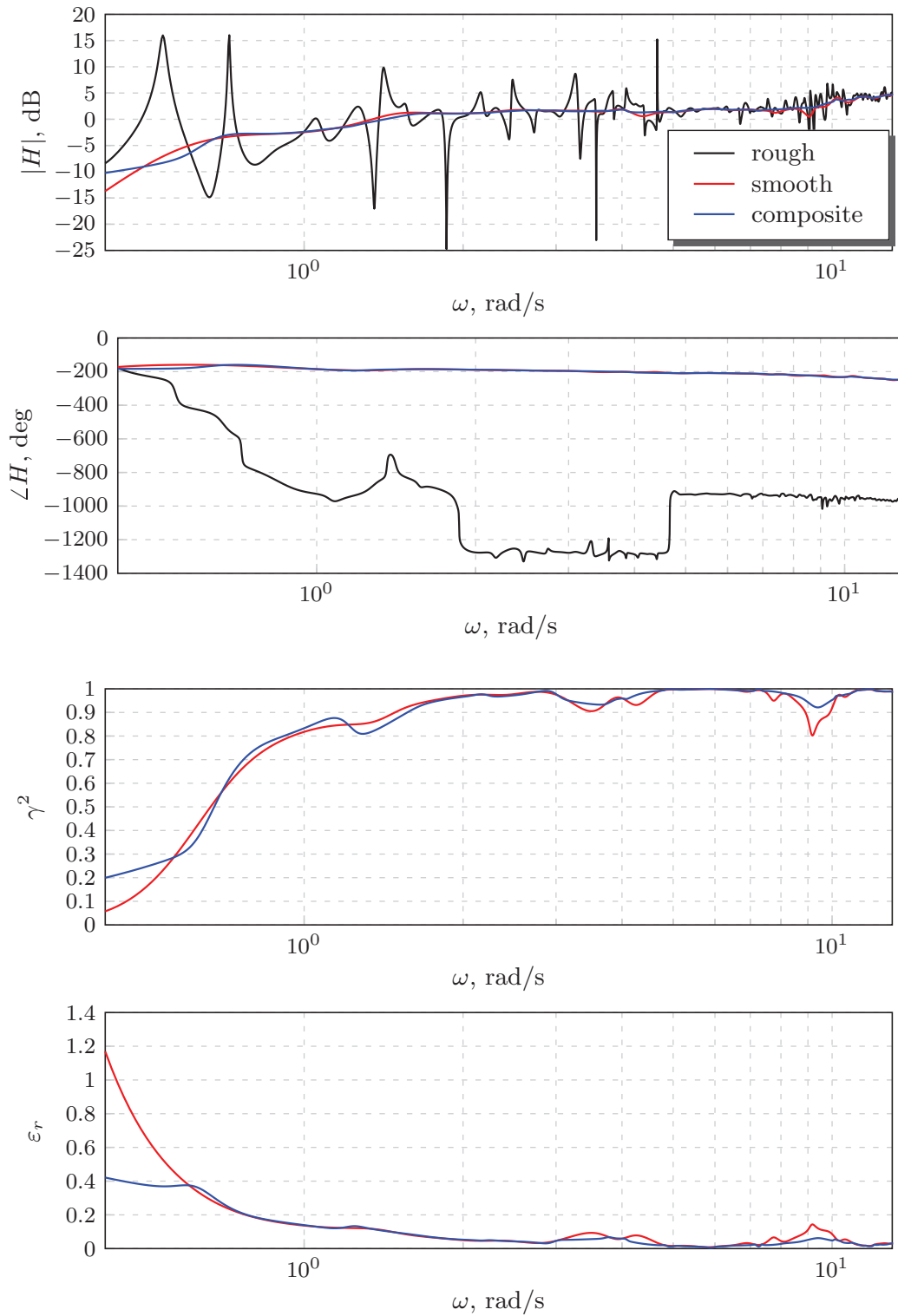


Figure 3.5: Estimated frequency-response function for pitch motion

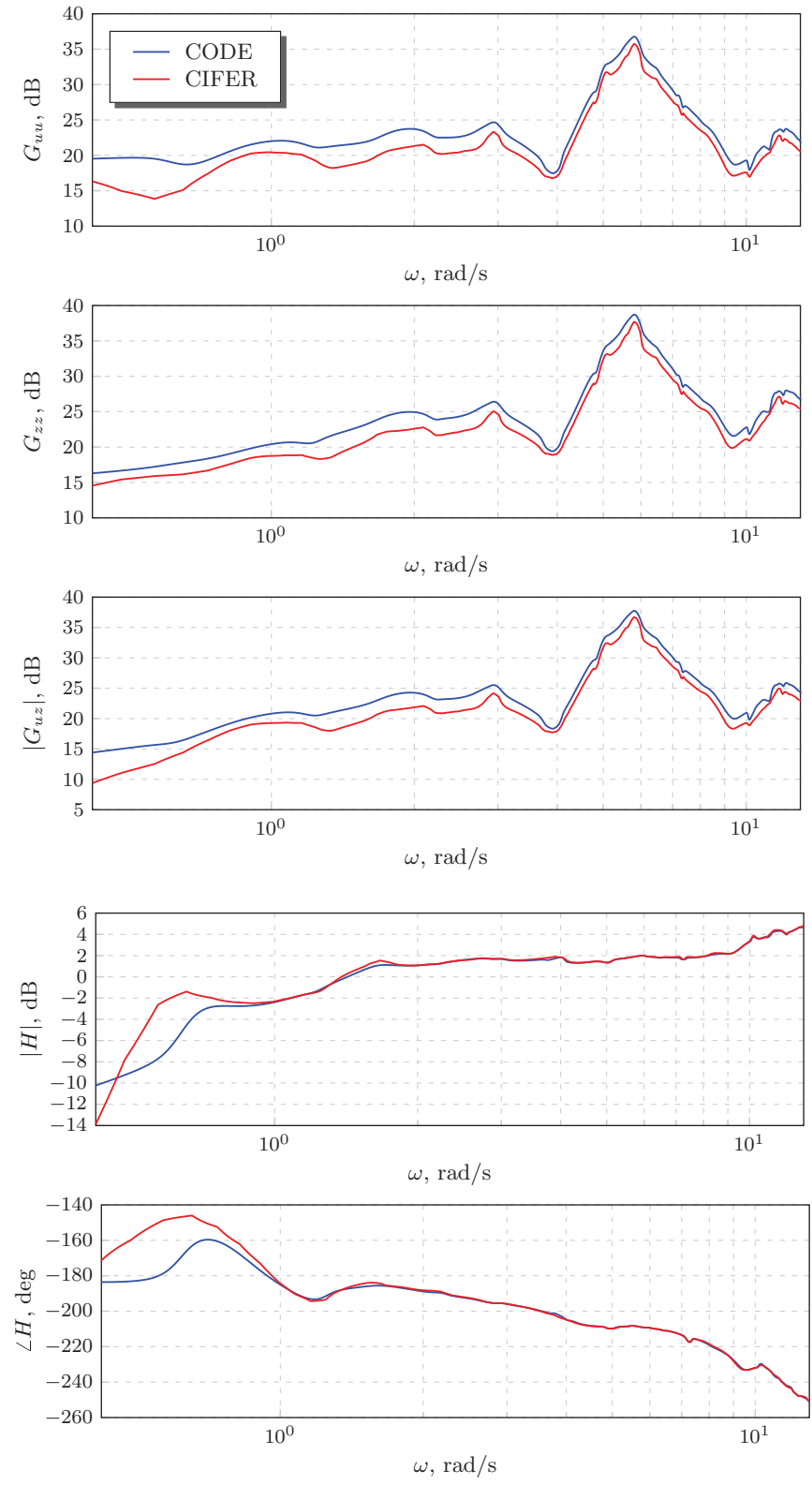


Figure 3.6: Identification results for longitudinal mode

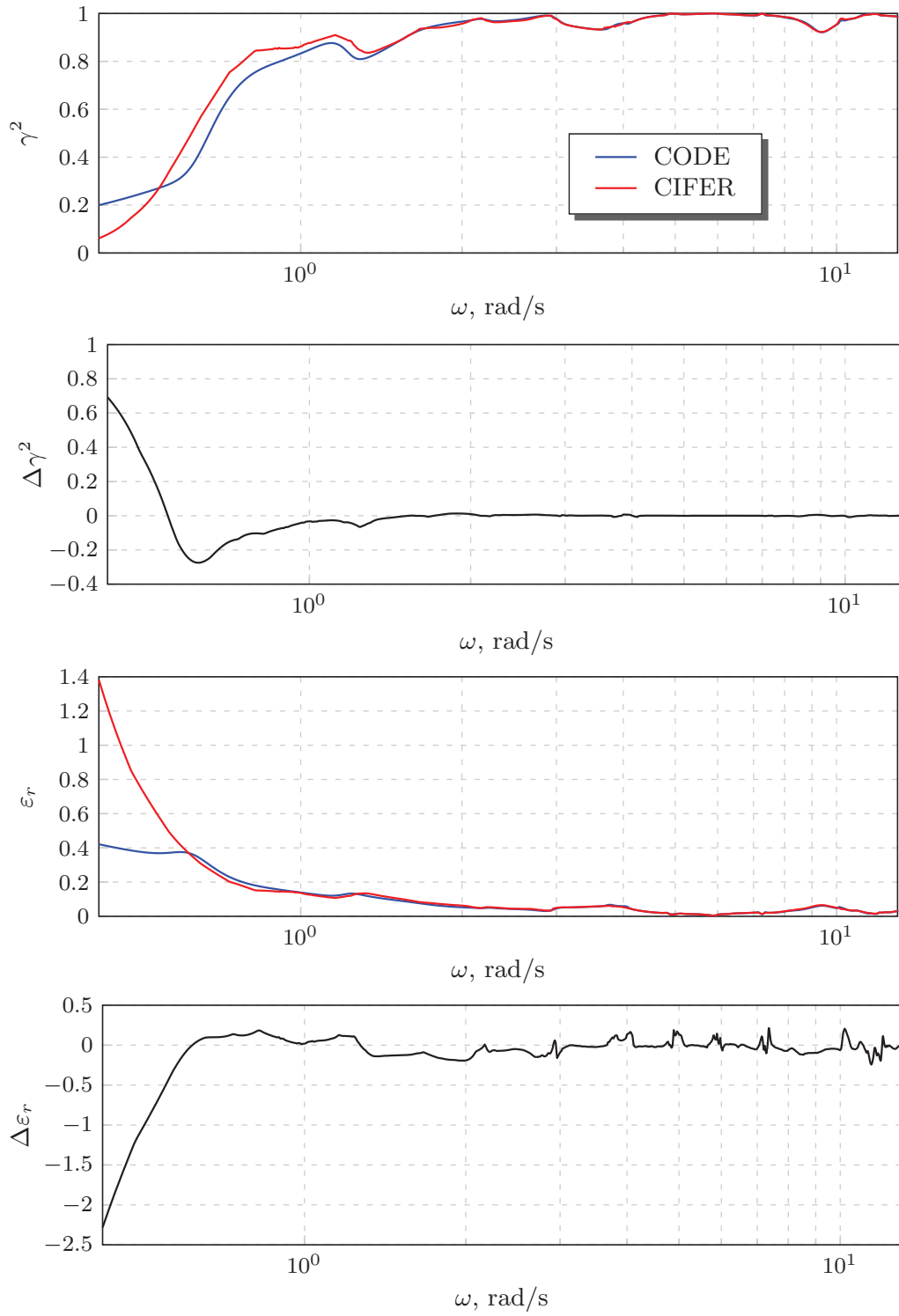


Figure 3.7: Accuracy metrics for longitudinal mode identification

3.4.2 Lateral Dynamics

The dataset used for the identification of lateral mode consists of lateral cyclic δ_{lat} as the input, and roll-rate p as the output. The spectral functions, i.e. input, output, and cross-PSDs for lateral roll mode are illustrated in Fig. 3.8. The results for frequency-response estimation in form of a Bode plot are depicted in Fig. 3.9, along with the corresponding accuracy metrics. Figure 3.10 shows the identification results obtained from the developed code and CIFER. Figure 3.11 provides the accuracy measures to be used for validating each identified model, and comparing the results with one another.

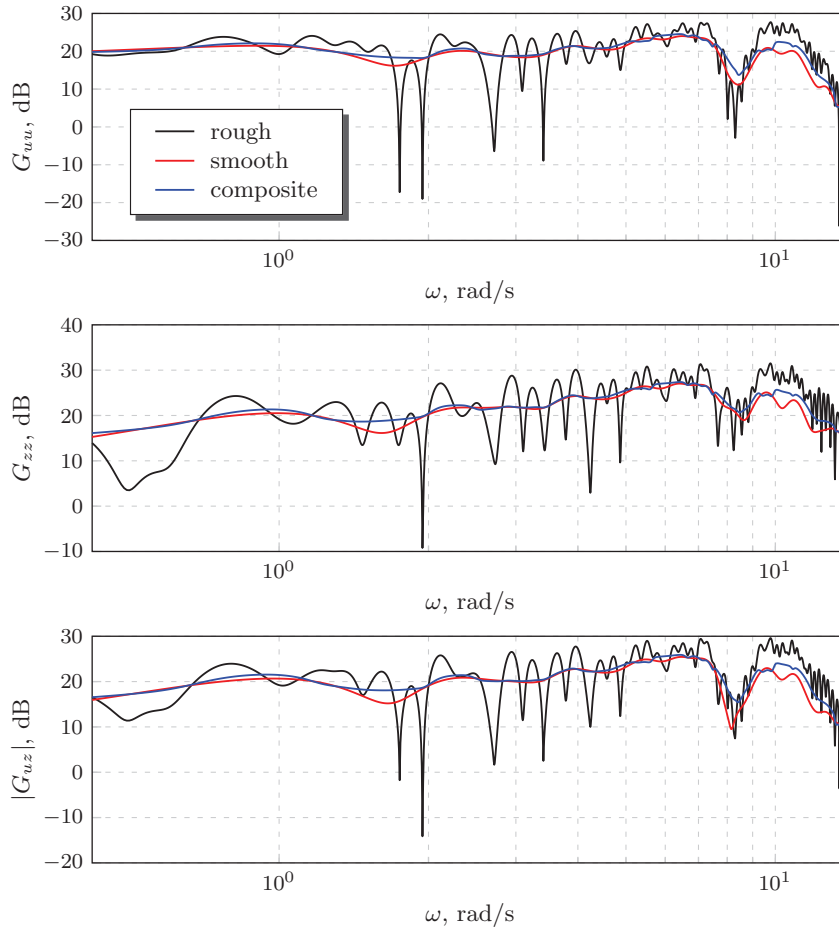


Figure 3.8: Estimated spectral functions for roll motion

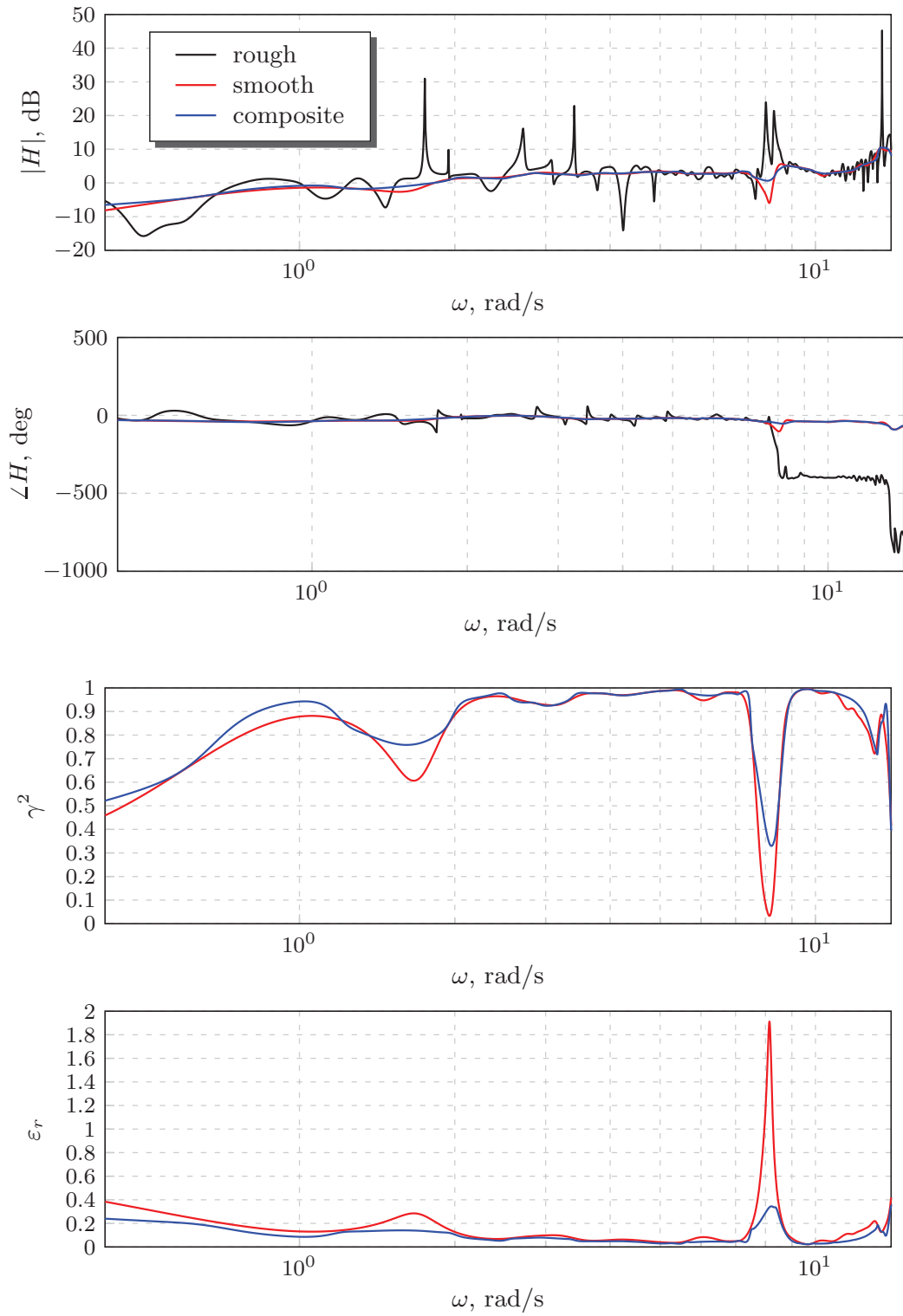


Figure 3.9: Estimated frequency-response function for roll motion

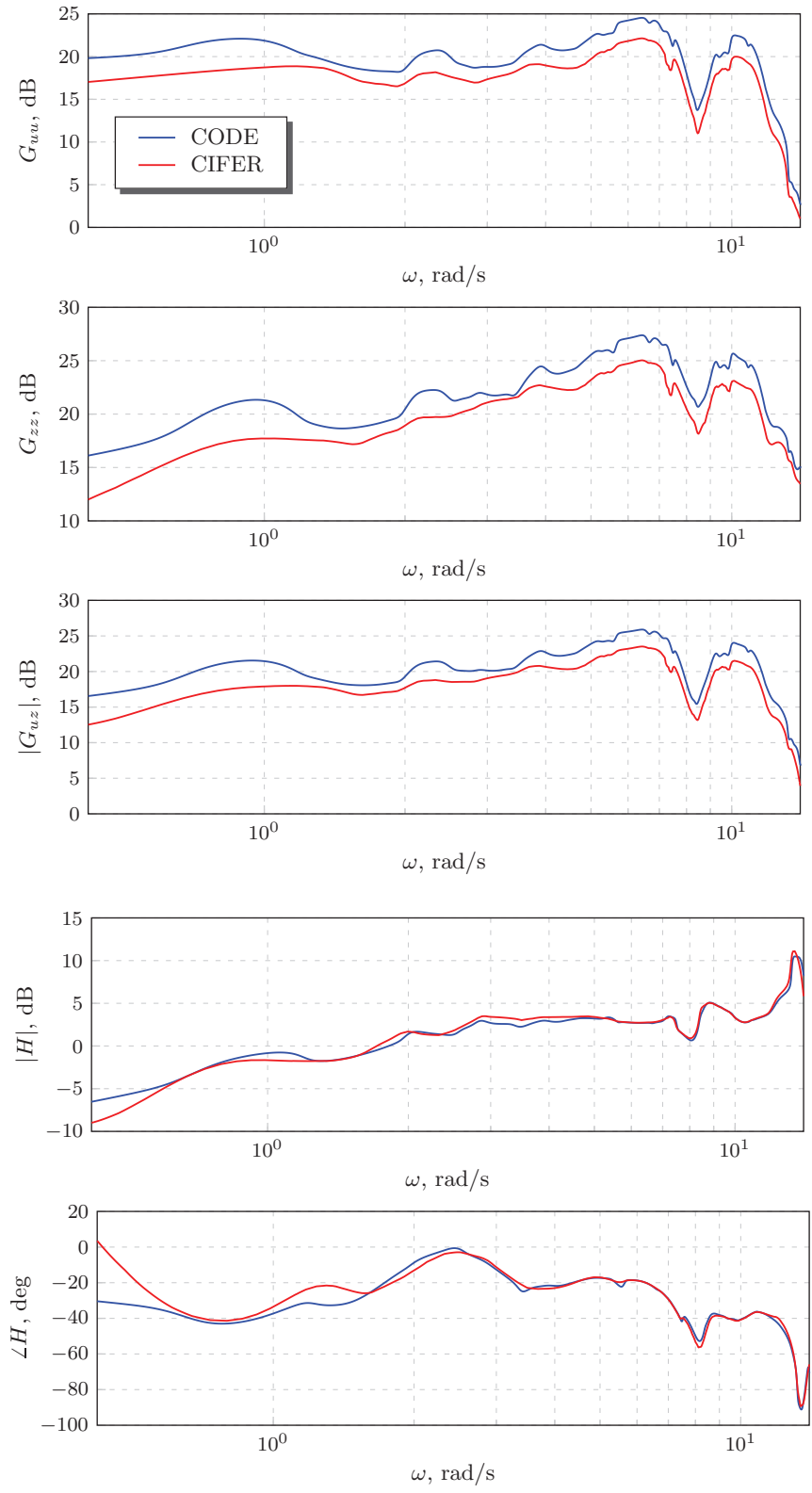


Figure 3.10: Identification results for lateral mode

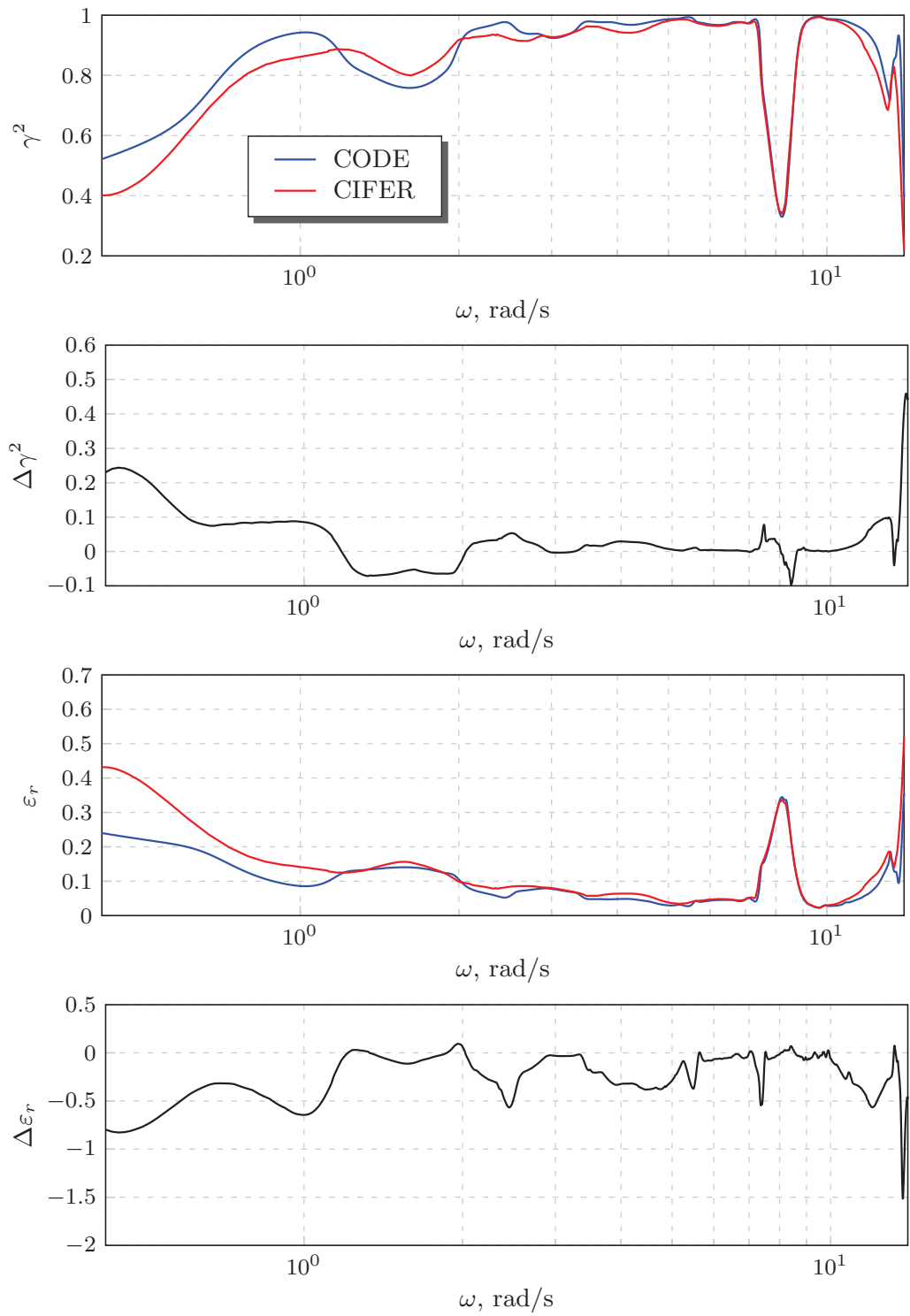


Figure 3.11: Accuracy metrics for lateral mode identification

3.5 Analysis and Discussion

As a general rule of thumb, $\gamma^2 \geq 0.6$ and $\varepsilon_r \leq 0.2$ demonstrate acceptable accuracy in frequency-response estimation [12]. It is worth mentioning that in the method used for rough estimation of the frequency-response function, which can be also interpreted as a windowing technique with one rectangular window ($T_{win} = T_{rec}$), coherence function gives a meaningless value of 1 for all frequency points. So, the coherence function and random error estimation are only considered as accuracy measures when a non-rectangular windowing technique is utilized.

Firstly, we consider the comparison between the results of three different techniques exploited for frequency-response identification. For both longitudinal and lateral dynamics, the PSD plots of Figs. 3.4 and 3.8 show the superiority of the smooth and the composite spectral estimates over the rough estimation of spectral functions. It can be translated into the ability of the windowing techniques in eliminating the effects of random noise in spectral estimates. In magnitude plots of Figs. 3.5 and 3.9, the rough estimation results follow the trend of two other techniques with some fluctuations. However, for the phase plots of the same figures, the rough estimation is unable to provide an acceptable estimate.

In order to compare the smooth and composite estimations of the frequency-response function, we can refer to the accuracy metric plots of Figs. 3.5 and 3.9, for longitudinal and lateral dynamics, respectively. For the pitch motion, in frequency range of 1 – 2 rad/s, the overlapped windowing gives a slightly better result. For everywhere else in the spectrum, composite windowing provides more accuracy, i.e. more coherence and less random error. For the roll motion, composite windowing is superior throughout the whole spectrum, and is significantly better in frequency ranges of 0.3 – 2 and 7 – 9 rad/s. Hence, for both dynamic modes, identified models obtained from the composite windowing technique are more reliable, hence chosen for comparison with CIPHER identified models.

Next, we compare the non-parametric models acquired from the developed SID tool and CIPHER. The PSD plots for both dynamic modes depict a systematic error between our results and CIPHER's, as can be seen in Figs. 3.6 and 3.10. In the magnitude and phase plots of the same figures, the results of both tools closely follow one another in mid and high frequencies (frequency range of 1 – 12 rad/s); however, there is a considerable offset between low frequency results (frequency range of 0.3 – 1 rad/s).

In order to verify the fidelity of the identified models, we refer to the accuracy metrics of Figs. 3.7 and 3.11, for longitudinal and lateral modes, respectively. For longitudinal dynamics, our results are more accurate in 0.3 – 0.5 rad/s, and CIPHER gives better results in 0.5 – 2 rad/s. For the mid and high frequencies (frequency range of 2 – 12 rad/s) the results are only slightly different as can be seen in near-zero values for $\Delta\gamma^2$ and $\Delta\varepsilon_r$ in that spectrum. For lateral dynamics, however, the code provides higher coherence and lower random error in low and high frequencies (0.3 – 1 and 2 – 12 rad/s), and CIPHER results are inferior except for the range of 1 – 2 rad/s.

Overall, the acceptable accuracy is achieved in the frequencies beyond 0.7 rad/s for the longitudinal mode, and 0.4 rad/s for the lateral mode. The coherence function and random error estimations for lateral dynamics in the range of 7 – 9 rad/s are way beyond the acceptable range, which can be seen essentially in the poor excitation of lateral cyclic input. According to the accuracy measures, and based on the comparison with CIPHER, it can be concluded that the developed Matlab code can successfully estimate accurate non-parametric models for longitudinal and lateral dynamics of Trex-700 in almost entire frequency range of interest.

Chapter 4

Parametric Model Identification

This chapter addresses the techniques required for acquiring a minimal adequate parametric model for dominant dynamics of the UAV helicopter testbed, Align Trex-700, from flight test data. Previously, in Chapter 3, a non-parametric model identification method was examined to find an unbiased estimate of the frequency-response function for longitudinal and lateral dynamics. Similar to Chapter 3, the parametric modeling techniques of this chapter are implemented in a SISO frequency-domain identification for on-axis longitudinal and lateral responses.

This chapter is organized as follows. The opening Section 4.1 gives a brief explanation for parametric model identification. Section 4.2 introduces Low Order Equivalent System (LOES) model identification as a type of parametric identification approach. Section 4.3 reviews first-principle modeling techniques used for developing a proper model structure to capture the flight dynamics of small-scale helicopters. In Sections 4.4 and 4.5, two parameter estimation techniques, plus two proposed solution routines will be described from a theoretical point of view. Section 4.6 contains parametric model identification results for Trex-700. The last Section 4.7 concludes this chapter.

4.1 Introduction

Parametric model identification of an aircraft aims to find an accurate and reliable estimate of the unknown parameters, i.e. aerodynamic derivatives, based on which the linear aircraft equations of motion are formulated. This can be implemented in frequency-domain by fitting a known model structure with unknown parameters to the frequency-domain transformation of the measured input-output data. The identification problem can be degraded to a parameter estimation problem if the model structure, whether a state-space formulation or a transfer function representation, is known *a priori*. The state-space formulation is dominantly used for finding a complete model, including most of the aerodynamic derivatives, typically in a MIMO identification procedure. A transfer function formulation, however, attempts to estimate the key parameters of major dynamic modes, and mostly used in a SISO model identification [10, 12].

4.2 LOES Modeling

LOES modeling is a type of transfer function modeling which attributes system input and output with a linear relation, including an exponential delay term associated with the input. The concept of LOES was introduced originally in the 1970s for aircraft handling quality purposes, where a low order transfer function was fitted to a high-order frequency-response obtained from a high-order system [29]. An extension of LOES models was later implemented in parametric system identification of flight vehicles with a similar approach, in addition to including nonlinearities as well as high-order effects in the delay term. A typical third-order LOES model is shown in equation (4.1):

$$T(s) = \frac{b_0s^2 + b_1s + b_2}{a_0s^3 + a_1s^2 + a_2s + a_3} e^{-\tau s}. \quad (4.1)$$

LOES modeling is considered as an intermediate step in the model identification of an aircraft, as it provides information about fundamental dynamic characteristics, and estimates parameters associated with dominant dynamic modes. A comprehensive dynamic model, as an ultimate goal in modeling, accounts for all dynamic modes, and requires many measurements of the aircraft states. The significance of LOES models, however, lies in the ability to approximate a high-order complex aircraft response to pilot input with minimum adequate parameters in the form of a transfer function, which can be interpreted and analyzed more readily. Hence, they are found to be quite sufficient for a wide range of applications, such as aircraft development, subsystem modeling, structural mode determination, control law design validation, flight mechanics characterization, and simulation [10, 12].

The central task in LOES parametric model identification is to find a proper model structure for desired dynamic modes with physically meaningful parameters. The rest requires a parameter estimation technique to approximate those unknown parameters. However, the truncation of highly complex and coupled helicopter dynamics into a low order model requires a thorough knowledge about flight dynamics of rotorcraft, and is not an easy task. Hence, we need to shed light on principles of rotorcraft dynamics before we proceed. An overview of model development of small-scale helicopters, plus the model forms chosen for this work, are discussed in the next section.

4.3 Rotorcraft Dynamics

The dynamical behavior of a conventional helicopter is dominated by main and tail rotor systems, where aerodynamic forces and moments are produced and controlled through angular and aeroelastic movements of the rotating blades. The resulting

forces and moments will then act on the helicopter body, and cause the vehicle to translate and rotate simultaneously in six degrees of freedom. The main rotor blades are controlled through a swashplate mechanism which transmits the actuator movements, fixed to the body, to the blades revolving at a very high speed. The actuators are commanded by helicopter major controls, which consist of collective, longitudinal and lateral cyclic, and tail rotor inputs. Fig. 4.1 illustrates the swash plate mechanism of Align Trex-700 used as the testbed for this research work.



Figure 4.1: Swashplate mechanism of Align Trex-700, © MicroPilot

The rotor system actuators aim to adjust pitch angle of the blades. The pitch angle, also referred to as feathering angle, is the rotation of the blade around its span. An increase in the pitch angle causes the rotating blades to face the air at a relatively higher angle of attack and increases the lift accordingly. The collective control apply the same pitch angle to all the blades simultaneously, and is the primary source of lift and thrust forces. The cyclic controls adjust the pitch angle of the main rotor blades different from one another in order to produce longitudinal and lateral moments.

The tail rotor control regulates the pitch angle of the tail rotor blades similar to the collective control in order to generate directional moment.

The helicopter responds to the controls in a multi-axis behavior, where a single-axis control can change the position and attitude in multiple axes. Yet, a significant weight of the controls is given to *on-axis* dynamics¹. The rotor system also reacts to the main rotor controls by adjusting coning and tilting angles of the rotor disk (also referred to as tip-path plane) in multiple harmonics. Fig. 4.2 shows a schematic view for the dominant harmonic of the rotor system response to the controls.

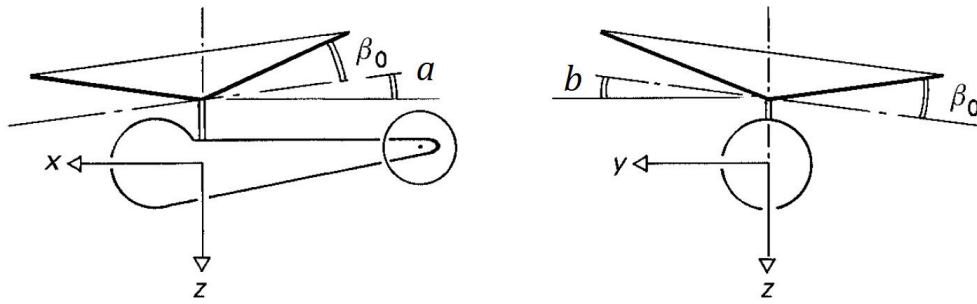


Figure 4.2: Rotor blades flapping motion [4]

4.3.1 Rigid-Body Model

A mathematical expression for helicopter flight dynamics can be developed from first principles where the aircraft is modeled using fundamental laws of mechanics such as Newton-Euler equations [4, 36, 37]. The nonlinear model obtained from generic equations of motion is comprised of translational and rotational dynamics of the rigid-body, which is exposed to external forces and moments due to aerodynamics, propulsion, and gravity. The key task in identification of the model for flight vehicles is finding an accurate expression for aerodynamic forces and moments in terms of aircraft dynamic and control variables [38]. The collected equations of motion

¹On-axis responses for collective, longitudinal and lateral cyclic, and tail rotor inputs are considered as vertical velocity, longitudinal, lateral, and directional attitudes, respectively.

for rigid-body dynamics of a small-scale conventional helicopter are given in equations (4.2) to (4.10). These equations are derived with respect to the inertial reference frame, with the principal variables expressed in a body-fixed reference frame located at the center of gravity of the vehicle. Fig. 4.3 depicts body axes x, y, z , velocities u, v, w , angular rates p, q, r , and external forces and moments, X, Y, Z and L, M, N , respectively.

Translational Dynamics:

$$\dot{u} = (-wq + vr) + X/m - g\sin\theta \quad (4.2)$$

$$\dot{v} = (-ur + wp) + Y/m + g\cos\theta\sin\phi \quad (4.3)$$

$$\dot{w} = (-vp + uq) + Z/m + g\cos\theta\cos\phi \quad (4.4)$$

Rotational Dynamics:

$$\dot{p} = -qr(I_{yy} - I_{zz})/I_{xx} + L/I_{xx} \quad (4.5)$$

$$\dot{q} = -pr(I_{zz} - I_{xx})/I_{yy} + M/I_{yy} \quad (4.6)$$

$$\dot{r} = -pq(I_{xx} - I_{yy})/I_{zz} + N/I_{zz} \quad (4.7)$$

Rotational Kinematics:

$$\dot{\phi} = p + \tan\theta(q\sin\phi + r\cos\phi) \quad (4.8)$$

$$\dot{\theta} = q\cos\phi - r\sin\phi \quad (4.9)$$

$$\dot{\psi} = \sec\theta(q\sin\phi + r\cos\phi) \quad (4.10)$$

In equations (4.2) to (4.10), ϕ, θ, ψ are Euler angles used for describing the angular orientation of the aircraft. The Euler angles refer to transformation from the inertial reference frame to the body-fixed frame in a specific sequence, i.e. yaw (ψ), pitch (θ), and roll (ϕ). Aircraft moments of inertia around the body axes are denoted as I_{xx}, I_{yy}, I_{zz} , and aircraft mass is denoted as m . The products of inertia, i.e. I_{xy}, I_{xz}, I_{yz} , are assumed to be small and therefore neglected [16].

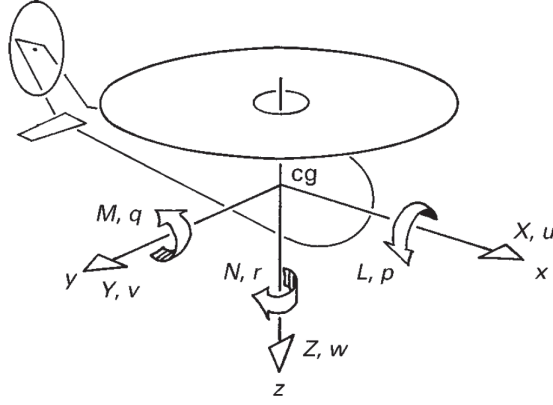


Figure 4.3: Helicopter body-fixed frame [4]

4.3.2 Extension of the Rigid-Body Model

The six Degree-Of-Freedom (6 DOF) rigid-body model does not suffice for capturing the rotorcraft flight dynamics completely. Higher order effects, mostly due to rotor blades aeroelasticity, must be considered in order to improve the model fidelity. A well-known extension of the 6 DOF model, which accounts for simplified rotor dynamics in addition to the rotor-body couplings, is called *hybrid model* [39]. The hybrid model, which was originally developed for full-scale helicopters, was adopted for model-scale rotorcrafts by Mettler [16]. This model aims to capture the dominant dynamic modes of the rotor system by modeling the blades flapping motion through the tilt angles of the tip-path-plane in the longitudinal and lateral directions, denoted as a and b , respectively (see Fig. 4.2). This model is presented in following equations:

Simplified Rotor Dynamics:

$$\dot{a} = \frac{-\gamma\Omega}{16}a + \frac{k_\beta}{2\Omega I_\beta}b - q + \frac{\gamma}{16}p - \Theta_a \quad (4.11)$$

$$\dot{b} = \frac{-\gamma\Omega}{16}b - \frac{k_\beta}{2\Omega I_\beta}a - p - \frac{\gamma}{16}p + \Theta_b \quad (4.12)$$

where I_β is the moment of inertia of the blade about the flapping hinge, k_β is the flapping hinge restraint spring constant, γ is the blade Lock number, Ω is the rotor speed, and Θ_a and Θ_b are the blade pitch/feathering angles in longitudinal and

lateral directions, respectively.

Along with modeling the rigid-body and the rotor dynamics, a feedback system which is commonly used to augment the stability of the yaw channel has to be modeled. It is quite well known that the yaw dynamics of rotorcrafts with tail rotor configuration is highly sensitive to controls (see equation (4.7)). This is mainly due to the large size of the tail beam, where small changes in rotational speed of the main rotor, or pitch angle of the tail-rotor blades can produce a huge yawing moment (N). This sensitivity is even more extreme for unmanned helicopters with faster dynamics and smaller size, which makes their manual control quite challenging. Hence, it is essential for most of small-scale helicopters to be equipped with a yaw-rate gyro in order to enhance their yaw stability and handling qualities [24]. A simple first-order model is used to capture the effect of this feedback system:

Yaw Damping System:

$$\dot{r}_{fb} = -K_{r_{fb}}r_{fb} + K_r r \quad (4.13)$$

where r_{fb} is the yaw rate gyro feedback, and $K_{r_{fb}}$ and K_r are the feedback gains.

4.3.3 Model Linearization

The aforementioned set of nonlinear equations (4.2) to (4.10) can be linearized around a reference/trim flight condition using *small disturbance theory*, where the states, forces, and moments of the system are replaced by small perturbations around their trim values [40]. For example, the vertical translational velocity w is replaced by Δw according to $w = w_0 + \Delta w$, in which w_0 refers to the trim vertical velocity. Hereafter, the Δ symbol is dropped from all variables for simplicity. Furthermore, the aerodynamic forces and moments, denoted as X, Y, Z and L, M, N respectively, can be expressed in terms of the aircraft states and control inputs by employing a linear *Taylor Series Expansion* [41]. The basic helicopter control variables consist of

the main rotor collective pitch δ_{col} , the tail rotor collective pitch δ_{ped} , the longitudinal cyclic input δ_{lon} , and the lateral cyclic input δ_{lat} . As an example, for the longitudinal moment component M one can get

$$M = \frac{\partial M}{\partial u} \delta u + \frac{\partial M}{\partial w} \delta w + \frac{\partial M}{\partial q} \delta q + \dots + \frac{\partial M}{\partial \delta_{lon}} \delta_{lon} + \dots \quad (4.14)$$

where the partial derivatives of M with respect to the states and controls are called stability and control derivatives, or aerodynamic derivatives, which are abbreviated as follows:

$$\frac{\partial M}{\partial \delta_{lon}} = M_{lon}. \quad (4.15)$$

It should be noted that not all of the states and controls contribute in each aerodynamic force and moment. Associating forces and moments to the variables by which they are altered is the principle of the parametric system identification, which is also referred to as model structure determination.

The complete linearized equations of motion for a flybarless small-scale helicopter is collected in a state-space form in equation (4.16). In this differential equation, the system matrix \mathbf{A} contains the stability derivatives, and the input matrix \mathbf{B} contains control derivatives. Also, \mathbf{x} and \mathbf{u} are state and input vectors, respectively.

$$\dot{\mathbf{x}} = \mathbf{A}\mathbf{x} + \mathbf{B}\mathbf{u} \quad (4.16)$$

where the state vector is

$$\mathbf{x} = [u, v, w, p, q, r, \phi, \theta, a, b, r_{fb}]^T \quad (4.17)$$

and the input vector is

$$\mathbf{u} = [\delta_{lat}, \delta_{lon}, \delta_{ped}, \delta_{col}]^T \quad (4.18)$$

$$\mathbf{A} = \left[\begin{array}{ccc|ccc|cc|cc|c}
X_u & 0 & 0 & 0 & 0 & 0 & 0 & -g & X_a & 0 & 0 \\
0 & Y_v & 0 & 0 & 0 & 0 & g & 0 & 0 & Y_b & 0 \\
0 & 0 & Z_w & 0 & 0 & Z_r & 0 & 0 & Z_a & Z_b & 0 \\
\hline
L_u & L_v & 0 & 0 & 0 & 0 & 0 & 0 & 0 & L_b & 0 \\
M_u & M_v & 0 & 0 & 0 & 0 & 0 & 0 & M_a & 0 & 0 \\
0 & N_v & N_w & N_p & 0 & N_r & 0 & 0 & 0 & 0 & N_{r_{fb}} \\
\hline
0 & 0 & 0 & 1 & 0 & 0 & 0 & 0 & 0 & 0 & 0 \\
0 & 0 & 0 & 0 & 1 & 0 & 0 & 0 & 0 & 0 & 0 \\
\hline
0 & 0 & 0 & 0 & -1 & 0 & 0 & 0 & \frac{-1}{\tau_f} & \frac{A_b}{\tau_f} & 0 \\
0 & 0 & 0 & -1 & 0 & 0 & 0 & 0 & \frac{B_a}{\tau_f} & \frac{-1}{\tau_f} & 0 \\
\hline
0 & 0 & 0 & 0 & 0 & K_r & 0 & 0 & 0 & 0 & K_{r_{fb}}
\end{array} \right] \quad (4.19)$$

$$\mathbf{B} = \left[\begin{array}{cc|cc}
0 & 0 & 0 & 0 \\
0 & 0 & 0 & 0 \\
0 & 0 & 0 & Z_{col} \\
\hline
0 & 0 & 0 & 0 \\
0 & 0 & 0 & 0 \\
0 & 0 & N_{ped} & N_{col} \\
\hline
0 & 0 & 0 & 0 \\
0 & 0 & 0 & 0 \\
\hline
\frac{A_{lat}}{\tau_f} & \frac{A_{lon}}{\tau_f} & 0 & 0 \\
\frac{B_{lat}}{\tau_f} & \frac{B_{lon}}{\tau_f} & 0 & 0 \\
\hline
0 & 0 & 0 & 0
\end{array} \right] \quad (4.20)$$

This formulation is originally developed by Mettler [15] for model identification of Yamaha R-50 helicopter in hover flight regime. A similar model for cruise flight

regime is also addressed in reference [15]. This realization of rotorcraft dynamics showed promise for modeling various model-scale helicopters as it is used extensively in recent literature [1, 7, 14, 18–20, 42, 43]. Other quantification of helicopter linearized model accounting for higher order effects, such as rotor inflow dynamics, blade lead-lagging motion, and stabilizer bar dynamics can be found in references [8, 22, 44, 45]. The resulting simplified model is considered as local model, since it is only valid for the specific flight condition about which the model is linearized. A general linear model can be obtained by developing multiple set of local models in order to cover the entire flight envelope [16].

4.3.4 LOES Model Structure

As mentioned earlier, the LOES identification of on-axis dynamics for our target vehicle is desired in this chapter. With the insight gained from analytic modeling of helicopter dynamics in Section 4.3, we are now able to determine physically meaningful model structures for on-axis responses due to controls. Once the model structure is established, in other words, once the decision about the inclusion of the effective aerodynamic derivatives has been made, the model identification problem simply becomes a parameter estimation problem. The on-axis dynamics for a conventional helicopter composed of:

- **Heave mode:** Vertical velocity to main rotor collective, w/δ_{col}
- **Dutch-roll mode:** Roll-rate response to lateral cyclic, p/δ_{lat}
- **Short-period mode:** Pitch-rate response to longitudinal cyclic, q/δ_{lon}
- **Yaw mode:** Yaw-rate response to tail rotor collective, r/δ_{ped}

In order to obtain transfer function representation of these dynamic modes, we require to further simplify the fully coupled hybrid model of equation (4.16), which describes the fuselage, rotor, and feedback system dynamics. This can be

accomplished if two major assumptions are made. First, we assume that airflow around the rotor blades is quasi-steady². This will allow us to break down the rotor dynamics into transient and steady-state responses. We will then include the rotor transient dynamics in an equivalent time delay associated with inputs, denoted as τ . Moreover, the rotor steady-state dynamics will be modeled as *equivalent* stability and control derivatives of the rigid-body [15].

The other assumption for simplifying the model of equation (4.16) is neglecting cross-axis coupling in the rigid-body equations, and splitting them into longitudinal and lateral/directional dynamics [12]. The resulting decoupled models are a good approximation for capturing the dominant dynamic modes of the helicopter. It is worth recalling that, during the identification flight experiment, the pilot commands one control input at a time. The secondary controls will be kept in the lowest allowable amplitude not to correlate on-axis and off-axis responses with one another. In other words, except for the primary control and response, the rest of aircraft states and controls will have small variations. Therefore, the terms corresponding to off-axis dynamics can be dropped and the equations can be decoupled.

The longitudinal dynamics are described with state vector \mathbf{x}_{lon} , and control vector \mathbf{u}_{lon} in equation (4.21). Similarly, the lateral/directional dynamics are expressed with state vector \mathbf{x}_{lat} , and control vector \mathbf{u}_{lat} in equation (4.22). System matrices \mathbf{F}_{lon} and \mathbf{F}_{lat} , and input matrices \mathbf{G}_{lon} and \mathbf{G}_{lat} , contain the *equivalent* aerodynamics derivatives for longitudinal and lateral modes.

$$\dot{\mathbf{x}}_{lon} = \mathbf{F}_{lon}\mathbf{x}_{lon} + \mathbf{G}_{lon}\mathbf{u}_{lon} \quad (4.21)$$

$$\dot{\mathbf{x}}_{lat} = \mathbf{F}_{lat}\mathbf{x}_{lat} + \mathbf{G}_{lat}\mathbf{u}_{lat} \quad (4.22)$$

²Quasi-steady flow assumes that the airflow around the aircraft, as a result the aerodynamic forces and moments, change instantaneously when the flight vehicle is disturbed from its trim condition [46].

where the state and control vectors are given as:

$$\mathbf{x}_{lon} = [u, w, q]^T \quad (4.23)$$

$$\mathbf{x}_{lat} = [v, p, r, r_{fb}]^T \quad (4.24)$$

$$\mathbf{u}_{lon} = [\delta_{lon}(t - \tau_p), \delta_{col}(t - \tau_h)]^T \quad (4.25)$$

$$\mathbf{u}_{lat} = [\delta_{lat}(t - \tau_r), \delta_{ped}(t - \tau_y)]^T \quad (4.26)$$

in which τ_p , τ_r , τ_y , and τ_h are equivalent time delay for pitch, roll, yaw, and heave motions. The system and input matrices are given in the following:

$$\mathbf{F}_{lon} = \begin{bmatrix} X_u & 0 & X_q \\ 0 & Z_w & 0 \\ M_u & 0 & M_q \end{bmatrix} \quad \mathbf{G}_{lon} = \begin{bmatrix} X_{lon} & 0 \\ 0 & Z_{col} \\ M_{lon} & 0 \end{bmatrix} \quad (4.27)$$

$$\mathbf{F}_{lat} = \begin{bmatrix} Y_v & Y_p & 0 & 0 \\ L_v & L_p & 0 & 0 \\ N_v & N_p & N_r & N_{r_{fb}} \\ 0 & 0 & K_r & K_{r_{fb}} \end{bmatrix} \quad \mathbf{G}_{lat} = \begin{bmatrix} Y_{lat} & 0 \\ L_{lat} & 0 \\ 0 & N_{ped} \\ 0 & 0 \end{bmatrix} \quad (4.28)$$

The transfer function form of the dominant dynamic modes are obtained by taking a Laplace Transform from equations (4.21) and (4.22).

Heave Mode:

$$\frac{w}{\delta_{col}} = \frac{Z_{col}}{s - Z_w} e^{-\tau_2 s} \quad (4.29)$$

Short-Period Mode:

$$\frac{q}{\delta_{lon}} = \frac{(M_{lon})s + (X_{lon}M_u - M_{lon}X_u)}{s^2 - (X_u + M_q)s + (M_qX_u - X_qM_u)} e^{-\tau_1 s} \quad (4.30)$$

Dutch-Roll Mode:

$$\frac{p}{\delta_{lat}} = \frac{(L_{lat})s + (Y_{lat}L_v - L_{lat}Y_v)}{s^2 - (Y_v + L_p)s + (L_pY_v - Y_pL_v)} e^{-\tau_3 s} \quad (4.31)$$

Closed-Loop Yaw Mode:

$$\frac{r}{\delta_{ped}} = \frac{(N_{ped})s + (N_{ped}K_{r_{fb}})}{s^2 + (K_{r_{fb}} - N_r)s + (N_{r_{fb}}K_r - K_{r_{fb}}N_r)} e^{-\tau_4 s} \quad (4.32)$$

The LOES models of equations (4.29) to (4.32) give a meaningful representation of low order dynamics from a flight dynamics perspective. However, there are two problems associated with these models from estimation point of view. First, the second-order transfer functions are overparameterized, hence cannot be considered minimal adequate models. In other words, the information content in the measured flight data does not suffice for estimating all these parameters accurately. Second, there is high correlation between the parameters in the numerator and denominator of transfer functions. That is, in the estimation procedure, movement in one parameter can affect other parameter estimates significantly, which reduces the estimation accuracy. Some improvements can be achieved if we re-parameterize the second-order equations of pitch, roll, and yaw differently, as shown in the following [30]:

$$H = \frac{b_1 s + b_0}{s^2 + a_1 s + a_0} e^{-\tau s} \quad (4.33)$$

where the relation between the aerodynamic derivatives and new parameters of equation (4.33) is found by straightforward comparison. These model structures are in good agreement with the model structures suggested in references [12] and [22] for the same application. Moreover, as discussed in Chapter 3, the composite frequency-response estimates obtained from flight test data show a second-order behavior for pitch, roll, and yaw modes. The final characterization of the LOES models obtained for Align Trex-700 are listed in Table 4.1.

Table 4.1: LOES model structure for on-axis responses

Mode	$\mathbf{H}(s)$	LOES Model
Heave	$\frac{w}{\delta_{col}}$	$\frac{b_0}{s - a_0} e^{-\tau s}$
Dutch-Roll	$\frac{p}{\delta_{lat}}$	$\frac{b_0}{s^2 + a_1 s + a_0} e^{-\tau s}$
Short-Period	$\frac{q}{\delta_{lon}}$	$\frac{b_1 s + b_0}{s^2 + a_1 s + a_0} e^{-\tau s}$
Yaw	$\frac{r}{\delta_{ped}}$	

For simplicity, the same parameterization is used for all the transfer functions, as b_i for the numerator, a_i for the denominator, and τ for the exponential term. However, it is obvious that these parameters can be different in dimension and value.

4.4 Parameter Estimation Methods

The last step in the parametric identification is to estimate the unknown parameters in the postulated model structures. In the frequency-domain, this procedure involves a nonlinear parameter estimation, which should be solved with a nonlinear optimization technique. In this section, we will shed light on the theory of the parameter estimation methods used in this work. Moreover, a theoretical background is given for the nonlinear optimization routines which we employed to solve the estimation problem. First, a theoretical scheme is given for a general frequency-domain estimation problem. Then, the formulations for a specific SISO identification is presented. Finally, the derivations for the model structure of the short-period dynamics are obtained, due to its generality over other model structures presented in Table 4.1. The formulations for the other model forms can be simply derived following a similar procedure.

4.4.1 Maximum Likelihood Estimator

The nonlinear estimator used extensively in aircraft system identification is Maximum Likelihood estimator which is developed based on the *Fisher model* given as follows:

$$\mathbf{y} = \mathbf{h}(\boldsymbol{\theta}) + \boldsymbol{\nu} \quad (4.34)$$

where \mathbf{y} is measurement vector, i.e. the Fourier transform of the time-domain measured data, $\boldsymbol{\nu}$ is error vector which captures the model uncertainty, $\boldsymbol{\theta}$ is a vector of unknown parameters, and $\mathbf{h}(\boldsymbol{\theta})$ is the model structure which nonlinearly relates the model parameters to the measured data [10].

The maximum likelihood estimation is developed for a stochastic dynamic system described by differential equations with process noise. The solution of such an estimation problem requires a combination of a Kalman filter and a nonlinear parameter estimator. The Kalman filter is necessary because the states of the system are random variables and must be estimated. A nonlinear estimator is needed because the measurement and parameters are attributed by a nonlinear function, $\mathbf{h}(\boldsymbol{\theta})$.

For practical applications, a simplified version of maximum likelihood estimator is used, where an assumption of no process noise is made. The process noise can be neglected if the flight test is executed in calm air, and if the maneuvers are performed in a way to keep the linearity assumption of the model to be identified [10] (see Chapter 2). In such a case, the states can be calculated deterministically using simple algebraic calculations in the frequency domain, and there is no need for a Kalman filter.

The simplified maximum likelihood estimator assumes that the system to be identified is deterministic, and the input measurement data are free of noise; however, it accounts for the noise in the output measurements. The problem will be then reduced to the estimation of the unknown parameters of the known model structure, $\mathbf{h}(\boldsymbol{\theta})$. This can be done by minimizing a quadratic cost formulation obtained from

the concept of a likelihood function³ and given in the following equation:

$$J(\boldsymbol{\theta}) = n \sum_{k=0}^m \boldsymbol{\nu}_k^\dagger(\boldsymbol{\theta}) \mathbf{S}_{\nu\nu}^{-1} \boldsymbol{\nu}_k(\boldsymbol{\theta}) \quad (4.35)$$

where n and m are the number of data points in the time and frequency domains respectively, k is the frequency index, $\boldsymbol{\nu}_k(\boldsymbol{\theta})$ is the error vector given at each frequency point, $\boldsymbol{\nu}_k^\dagger(\boldsymbol{\theta})$ is the complex conjugate transpose of $\boldsymbol{\nu}_k(\boldsymbol{\theta})$, and $\mathbf{S}_{\nu\nu}^{-1}$ is a weighting matrix given as:

$$\hat{\mathbf{S}}_{\nu\nu} = \sum_{k=0}^m \boldsymbol{\nu}_k(\boldsymbol{\theta}) \boldsymbol{\nu}_k^\dagger(\boldsymbol{\theta}) \quad (4.36)$$

in which $\hat{\boldsymbol{\theta}}$ is an estimate of the vector of parameters $\boldsymbol{\theta}$. For the case of a SISO identification problem in this work, $n\mathbf{S}_{\nu\nu}^{-1}$ can be omitted from the cost without affecting the parameter estimation results, so the cost function can be reformulated as follows [30]:

$$J(\boldsymbol{\theta}) = \frac{1}{2} \sum_{k=0}^m |\nu_k(\boldsymbol{\theta})|^2 = \boldsymbol{\nu}^\dagger(\boldsymbol{\theta}) \boldsymbol{\nu}(\boldsymbol{\theta}) / 2 \quad (4.37)$$

In this work, two different approaches of the maximum likelihood estimator are used in order to estimate the LOES models of dominant dynamic modes, namely Output-Error (OE) method, and Frequency-response-Error (FE) method. In the following subsections the theoretical background for these two approaches will be discussed.

4.4.2 Output-Error Method

In the Fisher model of equation (4.34), if the measurement vector \mathbf{y} is the system output, the maximum likelihood estimator will minimize the sum of squared errors between the estimated and measured outputs, and the estimation is called Output-Error (OE) method [30]. For a known transfer function form \mathbf{H} , the output can be

³In Fisher estimation theory, the likelihood function is defined as the conditional probability density of the observation y , given the parameters $\boldsymbol{\theta}$, i.e. $L(y; \boldsymbol{\theta}) = p(y|\boldsymbol{\theta})$. The assumption of Gaussian distribution for the probability density $p(y)$ leads to the definition of a quadratic cost function for the maximum likelihood estimator [34].

estimated from the following:

$$\hat{\mathbf{z}} = \mathbf{H}(\hat{\boldsymbol{\theta}})\mathbf{u} \quad (4.38)$$

where \mathbf{u} is the Fourier coefficient vector of the measured input and $\hat{\mathbf{z}}$ is the vector of the estimated output. Then, the measurement equation can be formulated as:

$$\mathbf{z} = \hat{\mathbf{z}} + \boldsymbol{\nu} \quad (4.39)$$

where \mathbf{z} is the Fourier coefficient vector of the output measurements, and $\boldsymbol{\nu}$ is the error vector. Hence, the output error cost function can be given as:

$$J_{OE}(\boldsymbol{\theta}) = \frac{1}{2} \sum_{k=0}^m |z_k - \hat{z}_k|^2 \quad (4.40)$$

As an example, for the longitudinal short-period mode approximated by a second-order transfer function as given in Table 4.1, the pitch-rate estimate in terms of the unknown parameters is given as:

$$\hat{z}_k(\boldsymbol{\theta}) = \hat{q}_k(\boldsymbol{\theta}) = \left(\frac{b_1\omega j + b_0}{-\omega^2 + a_1\omega j + a_0} e^{-\tau\omega j} \right) \delta_{lon_k} \quad (4.41)$$

where $\boldsymbol{\theta} = [b_1, b_0, a_1, a_0, \tau]^T$ is the vector of the unknown parameters, ω is the frequency point at which the output is evaluated, and δ_{lon_k} is the Fourier coefficient of the measurements for longitudinal cyclic input. In a similar fashion, the output estimates can be developed for the other model forms of heave, roll, and yaw dynamics, as given in Table 4.1.

4.4.3 Frequency-Response-Error Method

Another derivation of the maximum likelihood estimator, which is the basis of the CIPHER transfer function identification package (namely NAVFIT) and has been extensively used in practice, attempts to adjust the unknown parameters by fitting the model to the estimated Bode plot of the measured input-output data [12]. The cost formulation used in this method is given as:

$$J_{FE}(\boldsymbol{\theta}) = \frac{20}{m} \sum_{k=0}^m w_k \left[\left(|H_k| - |\hat{H}_k(\boldsymbol{\theta})| \right)^2 + w_p \left(\angle H_k - \angle \hat{H}_k(\boldsymbol{\theta}) \right)^2 \right] \quad (4.42)$$

where $|H_k|$ and $\angle H_k$ are magnitude⁴ and phase of the calculated frequency-response from the spectral estimates (see Chapter 3), $|\hat{H}_k(\boldsymbol{\theta})|$ and $\angle \hat{H}_k(\boldsymbol{\theta})$ are magnitude and phase of the estimated transfer function, and w_k is a weighting function, all of which are evaluated at frequency index k . The weighting coefficient w_k depends upon the value of the coherence function of the calculated frequency-response, in order to emphasize the most reliable data (higher coherence) in the cost value. Also, w_p is a weighting constant used to balance the contributions of the magnitude and the phase in the cost function. The value for w_p and the expression for w_k are given in the following [12]:

$$w_p = 0.01745 \quad (4.43)$$

$$w_k = \left[1.58 \left(1 - e^{-\gamma_k^2} \right) \right]^2 \quad (4.44)$$

In this work, the composite frequency-response estimates obtained in Chapter 3 will be used for evaluating $|H_k|$ and $\angle H_k$ variables. The transfer function estimates $|\hat{H}_k(\boldsymbol{\theta})|$ and $\angle \hat{H}_k(\boldsymbol{\theta})$ are obtained from the model forms collected in Table 4.1 using complex algebra. As an example, magnitude and phase estimates of the second-order transfer function for the short-period mode can be written as:

$$|\hat{H}_k(\boldsymbol{\theta})| = 10 \log_{10} \frac{(b_1 \omega)^2 + b_0^2}{(a_0 - \omega^2)^2 + (a_1 \omega)^2} \quad (4.45)$$

$$\angle \hat{H}_k(\boldsymbol{\theta}) = -\tau \omega + \arctan \frac{b_1 \omega}{b_0} + \arctan \frac{a_1 \omega}{a_0 - \omega^2} \quad (4.46)$$

where $\boldsymbol{\theta} = [b_1, b_0, a_1, a_0, \tau]^T$ is the vector of the unknown parameters, and ω is the frequency point at which the output is evaluated. Similarly, the transfer function estimates can be developed for the other model forms of heave, roll, and yaw dynamics, as given in Table 4.1.

⁴The transfer function magnitude is expressed in dB, i.e. $H = 20 \log_{10}(z/u)$.

4.5 Nonlinear Estimation Routines

The nonlinear estimation methods derived from the maximum likelihood concept can be solved using any nonlinear optimization technique. Among all possible solution routines, two techniques are selected: Levenberg-Marquardt and Downhill Simplex, as they are found to have a high convergence rate for aircraft system identification applications [29, 34]. A quick theoretical background is given for these optimization techniques in this section.

4.5.1 Levenberg-Marquardt Solution

The Levenberg-Marquardt method is developed from the popular Newton-Raphson optimization technique. For a nonlinear estimator with unknown parameters vector $\boldsymbol{\theta}$, and cost function $J(\boldsymbol{\theta})$, the Newton-Raphson technique adjusts the parameters by minimizing the cost function in an iterative process. Firstly, a nominal value is considered for the parameters as $\boldsymbol{\theta}_0$. Next, the parameters are updated using the following equation:

$$\hat{\boldsymbol{\theta}} = \boldsymbol{\theta}_0 + \Delta\hat{\boldsymbol{\theta}} \quad (4.47)$$

where $\Delta\hat{\boldsymbol{\theta}}$ is given by

$$\Delta\hat{\boldsymbol{\theta}} = - \left[\frac{\partial^2 J}{\partial \boldsymbol{\theta} \partial \boldsymbol{\theta}^T} \Big|_{\boldsymbol{\theta}_0} \right]^{-1} \frac{\partial J}{\partial \boldsymbol{\theta}} \Big|_{\boldsymbol{\theta}_0} \quad (4.48)$$

The nominal value is then replaced by the parameter estimate ($\boldsymbol{\theta}_0 = \hat{\boldsymbol{\theta}}$) for the next iteration. The iterations will continue until some convergence criteria are satisfied [5]. The first-order gradient of the cost function denoted as $\partial J / \partial \boldsymbol{\theta}$ is called sensitivity matrix (\mathbf{S}), and the second-order gradient denoted as $\partial^2 J / \partial \boldsymbol{\theta} \partial \boldsymbol{\theta}^T$ is known as Fisher information or Hessian matrix (\mathbf{M}). The update equation can be also represented as the following:

$$\Delta\hat{\boldsymbol{\theta}} = - [\mathbf{M}|_{\boldsymbol{\theta}_0}]^{-1} \mathbf{S}|_{\boldsymbol{\theta}_0}. \quad (4.49)$$

The Levenberg-Marquardt method aims to augment the Newton-Raphson technique by improving the Hessian matrix in order to produce a more accurate inverse in the update equation (4.48). According to this technique, the Hessian matrix is augmented as:

$$\mathbf{M} = \mathbf{M}_0 + \lambda_l \mathbf{I} \quad (4.50)$$

where \mathbf{M}_0 is the original Hessian matrix, \mathbf{I} is the identity matrix, and λ_l is a positive nonzero scalar, initially set to $\lambda_l = 0.001$. This modification is implemented in a separate iterative procedure within the original iteration loop described with scrutiny in reference [5]. Typical convergence criteria for Levenberg-Marquardt technique involve one or more of the following:

- 1) Absolute values of the elements of the parameter update are small enough.
- 2) The elements in the cost gradient are close to zero.
- 3) Changes in the cost value for consecutive iterations are sufficiently small.

These criteria are quantified in the equations (4.51) to (4.53):

$$\left| (\hat{\theta}_j)_k - (\hat{\theta}_j)_{k-1} \right| < 1.0 \times 10^{-5} \quad \forall j, j = 1, 2, \dots, n_p \quad (4.51)$$

$$\left| (\partial J(\boldsymbol{\theta}) / \partial \theta_j)_{\boldsymbol{\theta} = \hat{\boldsymbol{\theta}}_k} \right| < 5.0 \times 10^{-2} \quad \forall j, j = 1, 2, \dots, n_p \quad (4.52)$$

$$\left| \frac{J(\hat{\boldsymbol{\theta}}_k) - J(\hat{\boldsymbol{\theta}}_{k-1})}{J(\hat{\boldsymbol{\theta}}_{k-1})} \right| < 0.001 \quad (4.53)$$

where n_p is the number of unknown parameters to be identified [10].

The accuracy of the estimation can be examined by evaluating the standard deviation of the estimated parameters. The standard deviation can be obtained from the diagonal elements of the covariance matrix, which follows the Cramer-Rao (CR) inequality as:

$$\text{Cov}(\hat{\boldsymbol{\theta}}) = E \left[(\hat{\boldsymbol{\theta}} - \boldsymbol{\theta})(\hat{\boldsymbol{\theta}} - \boldsymbol{\theta})^T \right] \geq \mathbf{M}^{-1} \quad (4.54)$$

where E is the operator for the expected value. In maximum likelihood method, the inverse Hessian matrix and the covariance matrix are attributable with scale factor of 5 to 10, accounting for non-Gaussian noise and modeling errors in the identification, as follows:

$$s_i = \sqrt{(\text{Cov}(\hat{\boldsymbol{\theta}}))_{ii}} = (5 \text{ to } 10)\sqrt{(\mathbf{M}^{-1})_{ii}} \quad \forall i = 1, \dots, n \quad (4.55)$$

where s_i is the standard deviation of the i th parameter, also known as Cramer-Rao bound [10]. It is usually evaluated in percentage of the identified parameter as the following:

$$\bar{s}_i = \overline{CR}_i = \left| \frac{CR_i}{\theta_i} \right| \times 100 \%. \quad (4.56)$$

In this work, we have applied Levenberg-Marquardt solution for solving the two aforementioned estimation techniques (OE and FE). For the OE method with the cost formulation given in equation (4.40), the Levenberg-Marquardt calculates the sensitivity and original Hessian matrices as:

$$\mathbf{S} = -\Re \left[\sum_{k=0}^m \frac{\partial \hat{z}_k}{\partial \boldsymbol{\theta}} v_k \right] \quad (4.57)$$

$$\mathbf{M}_0 = \Re \left[\sum_{k=0}^m \left(\frac{\partial \hat{z}_k}{\partial \boldsymbol{\theta}} \right)^\dagger \frac{\partial \hat{z}_k}{\partial \boldsymbol{\theta}} \right] \quad (4.58)$$

where \Re denotes the real elements in the first- and second-order gradients of the cost function, and \dagger is the denotation for complex conjugate transpose of a matrix with complex elements.

Likewise, for the FE estimation method with the cost function of equation (4.42), the Levenberg-Marquardt method provides the sensitivity and original Hessian matrices as:

$$\mathbf{S} = \frac{-40}{m} \sum_{k=0}^m w_k \left[\frac{\partial |\hat{H}_k|}{\partial \boldsymbol{\theta}} v_{m_k} + w_p \frac{\partial \angle \hat{H}_k}{\partial \boldsymbol{\theta}} v_{p_k} \right] \quad (4.59)$$

$$\mathbf{M}_0 = \frac{40}{m} \sum_{k=0}^m w_k \left[\left(\frac{\partial |\hat{H}_k|}{\partial \boldsymbol{\theta}} \right)^\dagger \frac{\partial |\hat{H}_k|}{\partial \boldsymbol{\theta}} + w_p \left(\frac{\partial \angle \hat{H}_k}{\partial \boldsymbol{\theta}} \right)^\dagger \frac{\partial \angle \hat{H}_k}{\partial \boldsymbol{\theta}} \right] \quad (4.60)$$

where v_{m_k} and v_{p_k} are the estimation error in magnitude and phase given as:

$$v_{m_k} = |H_k| - |\hat{H}_k(\boldsymbol{\theta})| \quad (4.61)$$

$$v_{p_k} = \angle H_k - \angle \hat{H}_k(\boldsymbol{\theta}) \quad (4.62)$$

The first-order gradient matrices of the estimated output ($\partial \hat{z}_k / \partial \boldsymbol{\theta}$) and the transfer function estimates ($\partial |\hat{H}_k| / \partial \boldsymbol{\theta}$ and $\partial \angle \hat{H}_k / \partial \boldsymbol{\theta}$), presented in equations (4.57) to (4.60), can be simply derived if the output equation and transfer function are known. In this work, we have calculated these gradients for the model structures given in Table 4.1. As an example, for the longitudinal short-period mode with output equation (4.41), the corresponding first-order gradient matrix takes the following form

$$\frac{\partial \hat{z}_k}{\partial \boldsymbol{\theta}} = \frac{\partial \hat{q}_k}{\partial \boldsymbol{\theta}} = \left[\frac{\partial \hat{q}_k}{\partial b_1}, \frac{\partial \hat{q}_k}{\partial b_0}, \frac{\partial \hat{q}_k}{\partial a_1}, \frac{\partial \hat{q}_k}{\partial a_0}, \frac{\partial \hat{q}_k}{\partial \tau} \right]. \quad (4.63)$$

If one takes all the derivatives, the resulting matrix will be:

$$\frac{\partial \hat{q}_k}{\partial \boldsymbol{\theta}} = \frac{\sigma_1}{\sigma_3} [j\omega, 1, j\omega\sigma_2/\sigma_3, \sigma_2/\sigma_3, -j\omega\sigma_2] \quad (4.64)$$

where σ_1 , σ_2 , and σ_3 are the collected forms of

$$\sigma_1 = \delta_{lon_k} e^{-\tau\omega j} \quad (4.65)$$

$$\sigma_2 = b_1\omega j + b_0 \quad (4.66)$$

$$\sigma_3 = -\omega^2 + a_1\omega j + a_0. \quad (4.67)$$

The derivations for the transfer function gradients are obtained similarly. Again, the formulation is derived for the longitudinal short-period mode as an example, with the transfer function magnitude and phase given in equations (4.45) and (4.46). The first-order gradients for the magnitude and the phase are found as:

$$\frac{\partial |\hat{H}_k|}{\partial \boldsymbol{\theta}} = \frac{20}{\ln 10} \left[\frac{b_1\omega^2}{\sigma_5}, \frac{b_0}{\sigma_5}, \frac{-a_1\omega^2}{\sigma_6}, \frac{-\sigma_4}{\sigma_6}, 0 \right] \quad (4.68)$$

$$\frac{\partial \angle \hat{H}_k}{\partial \boldsymbol{\theta}} = \left[\frac{\omega/b_0}{\sigma_7}, \frac{-b_1\omega/b_0^2}{\sigma_7}, \frac{-\omega/\sigma_4}{\sigma_8}, \frac{a_1\omega/\sigma_4}{\sigma_8}, -\omega \right] \quad (4.69)$$

where $\sigma_4, \sigma_5, \sigma_6, \sigma_7, \sigma_8$ are:

$$\sigma_4 = a_0 - \omega^2 \quad (4.70)$$

$$\sigma_5 = (b_1\omega)^2 + b_0^2 \quad (4.71)$$

$$\sigma_6 = (a_1\omega)^2 + \sigma_4^2 \quad (4.72)$$

$$\sigma_7 = (a_1\omega/\sigma_6)^2 + 1 \quad (4.73)$$

$$\sigma_8 = (b_1\omega/b_0)^2 + 1. \quad (4.74)$$

In an analogous fashion, the first-order gradients in equations (4.57) to (4.60) are calculated for other model structures as given in Table 4.1.

4.5.2 Downhill Simplex Solution

The other optimization routine employed in this work is called Downhill Simplex, also referred to as Simplex method. This technique is developed for minimization of a function that nonlinearly depends on more than one variable. It has a geometric basis, and it only requires function evaluation in its way to find the solution, i.e. no derivative is involved. Downhill Simplex method has a fast convergent rate among other nonlinear optimization routines, and is very efficient in terms of the function evaluations it needs [5].

In the nonlinear estimation problem, we have a vector of unknown parameters $\boldsymbol{\theta}$ with n_p elements, an initial guess $\boldsymbol{\theta}_0$, and an objective function or cost function $J(\boldsymbol{\theta})$ to be minimized. In order to solve this problem, the Simplex method defines a n_p -dimensional vector-space with $n_p + 1$ points or vertices. Each of these points corresponds to a vector of parameters. One of the vertices (does not matter which) takes the initial guess for parameters $\boldsymbol{\theta}_0$, and the other n_p vertices take the perturbed vector of parameters $\boldsymbol{\theta}_i$ determined as the following:

$$\boldsymbol{\theta}_i = \boldsymbol{\theta}_0 + d\boldsymbol{\theta}_i \quad i = 1, 2, \dots, n \quad (4.75)$$

where $d\boldsymbol{\theta}_i$ are perturbation matrices given as:

$$d\boldsymbol{\theta}_i(j) = \begin{cases} \lambda_s \boldsymbol{\theta}_0(j) & i = j \\ 0 & i \neq j \end{cases} \quad (4.76)$$

in which λ_s is the perturbation in percent, usually set to $\lambda_s = 0.01$, and $j = 1, 2, \dots, n_p$ is the parameter index. The Simplex method then evaluates the cost function at each vertex, and finds the minimum and maximum cost values (denoted as J_l and J_h) and their corresponding vertices (denoted as $\boldsymbol{\theta}_l$ and $\boldsymbol{\theta}_h$). The centroid of the points is also found from the following equation:

$$\bar{\boldsymbol{\theta}} = \frac{\sum_{k=0}^{n_p} \boldsymbol{\theta}_k}{n_p} \quad \forall k \neq h. \quad (4.77)$$

After all these initializations, the Simplex method starts an iterative loop in order to attain the minimum cost value. At each iteration, $\boldsymbol{\theta}_h$ is replaced by a new value after taking a series of steps in a specific sequence. There are four operations used in these steps, namely *reflection*, *expansion*, *contraction*, and *compression*. In the reflection, $\boldsymbol{\theta}_h$ is reflected with respect to the centroid by factor of $\alpha > 0$ and gives $\boldsymbol{\theta}_r$. In the expansion, $\boldsymbol{\theta}_r$ is expanded with respect to the centroid by factor of $\gamma > 1$ which yields to $\boldsymbol{\theta}_e$. In the contraction, $\boldsymbol{\theta}_h$ is contracted with respect to the centroid by factor of $0 < \beta < 1$ and delivers $\boldsymbol{\theta}_c$. Finally, in the compression, all the vertices are contracted along all dimensions towards the low point $\boldsymbol{\theta}_l$. These operations are quantified in equations (4.78) to (4.81).

$$\boldsymbol{\theta}_r = \bar{\boldsymbol{\theta}} - \alpha(\boldsymbol{\theta}_h - \bar{\boldsymbol{\theta}}) \quad (4.78)$$

$$\boldsymbol{\theta}_e = \bar{\boldsymbol{\theta}} + \gamma(\boldsymbol{\theta}_r - \bar{\boldsymbol{\theta}}) \quad (4.79)$$

$$\boldsymbol{\theta}_c = \bar{\boldsymbol{\theta}} + \beta(\boldsymbol{\theta}_h - \bar{\boldsymbol{\theta}}) \quad (4.80)$$

$$\boldsymbol{\theta}_i = (\boldsymbol{\theta}_i + \boldsymbol{\theta}_l)/2 \quad (4.81)$$

where α , β , γ are the algorithm coefficients with recommended values of $\alpha = 1$, $\beta = 0.5$, and $\gamma = 2$ [47]. The sequence in which these operations are performed is

discussed with scrutiny in references [5, 48]. In order to give a better understanding, the aforementioned operations are illustrated graphically in Fig. 4.4 for a typical three-dimensional simplex.

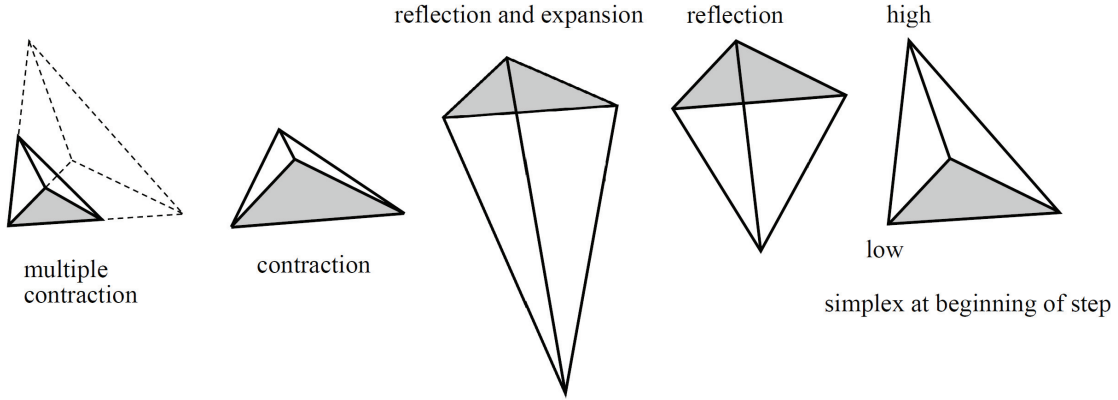


Figure 4.4: Possible outcomes of a step in Simplex method (adopted from [5])

At the end of the iteration, the new cost values are computed for the updated vertices, minimum and maximum cost values are found again, and a termination or convergence criteria is checked. The iterative loop is continued until the termination criteria is satisfied. A typical convergence criteria requires the relative difference between minimum and maximum cost value to be sufficiently small, that is:

$$\left| \frac{J_h - J_l}{J_h + J_l} \right| < 1.0 \times 10^{-8}. \quad (4.82)$$

In this work, the Downhill Simplex technique is utilized in order to find the parameter estimates which minimize the cost functions of equations (4.40) and (4.42) for short-period and roll model structures presented in Table 4.1. It is obvious that the Simplex method has less complexity in its formulation and computation burden compared to the Levenberg-Marquardt method introduced earlier.

4.6 Identification of the Model

The model identification problem was decreased to a nonlinear estimation problem after postulating a proper model structure in Section 4.3.4. For the transfer functions presented in Table 4.1, two nonlinear estimation problems are formulated, i.e. OE and FE, each of which is solved by employing two nonlinear optimization routines, i.e. Levenberg-Marquardt and Downhill Simplex. A Matlab code is generated for this reason. The Matlab program inputs the time-history data and delivers the identified LOES models. A schematic of the developed tool is represented in Fig. 4.5

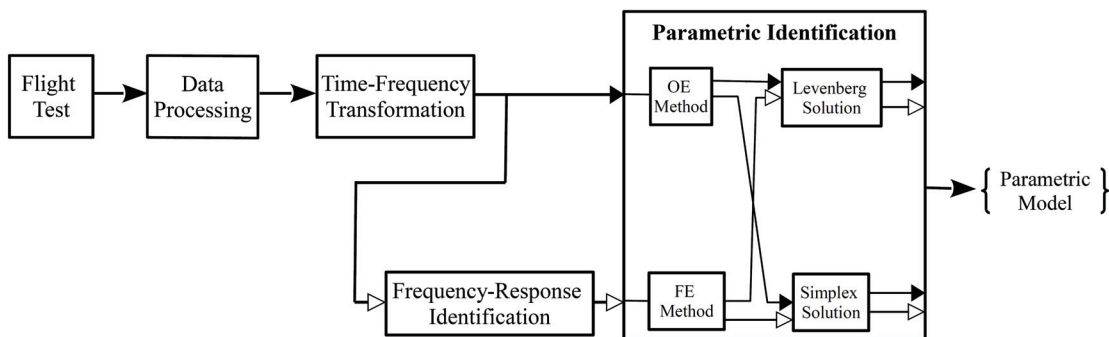


Figure 4.5: Schematic of the parametric SID tool

Beside identifying the models using our Matlab-based SID tool, the same time-history data are fed to CIPHER NAVFIT package for identifying another set of LOES models for comparison. Since the longitudinal and the lateral cyclic inputs are the only controls excited using frequency sweeps during the flight test, we are only able to identify the LOES models for short-period and roll modes. However, the Matlab code is quite capable for identifying the heave and yaw dynamics provided that the data is available. The Matlab package could be easily adapted for any transfer function form as well. In this section, we will provide the estimation results for longitudinal and lateral low order models, and compare them with the results obtained from CIPHER.

4.6.1 Longitudinal Dynamics

The parameters to be estimated are b_1 , b_0 , a_1 , a_0 , and τ from the transfer function given in Table 4.1. For the Levenberg solution, parameters τ and b_0 are fixed during the iterations. They are initially set to their corresponding values from CIPHER, however they are fine-tuned manually during multiple runs of the Matlab code. For the Simplex solution, the only parameter kept fixed is time delay τ .

The results of the OE method for the short-period mode is given in Table 4.2 which includes: estimated parameters, calculated modal characteristics (ζ and ω_n), and estimation final cost value for both Levenberg and Simplex solutions. Likewise, the FE estimation results are collected in Table 4.3, in addition to the results obtained from CIPHER. Figure 4.6 contains the pitch-rate estimates and measurements in both frequency-domain ($|\tilde{q}|$) and time-domain (q). Also, Fig. 4.7 depicts the Bode plot of the estimated model and measurement data, plus the time-domain verification of the estimated pitch-rate.

Table 4.2: Identification results: OE method for short-period dynamics

Symbols	Parameter Estimates	
	Levenberg	Simplex
b_1	-14.18	-10.07
b_0	-400.00	-391.07
a_1	12.63	9.99
a_0	368.22	406.36
τ	0.08	0.08
ζ	0.33	0.25
ω_n	19.19	20.16
J_{OE}	145.79	158.38

Table 4.3: Identification results: FE method for short-period dynamics

Symbols	Parameter Estimates		
	Levenberg	Simplex	CIFER [®]
b_1	-25.45	-10.05	-1.18
b_0	-400.00	-407.37	-566.60
a_1	15.28	10.04	9.41
a_0	390.19	394.15	451.69
τ	0.08	0.08	0.06
ζ	0.39	0.25	0.22
ω_n	19.75	19.85	21.25
J_{FE}	18.43	20.72	44.42

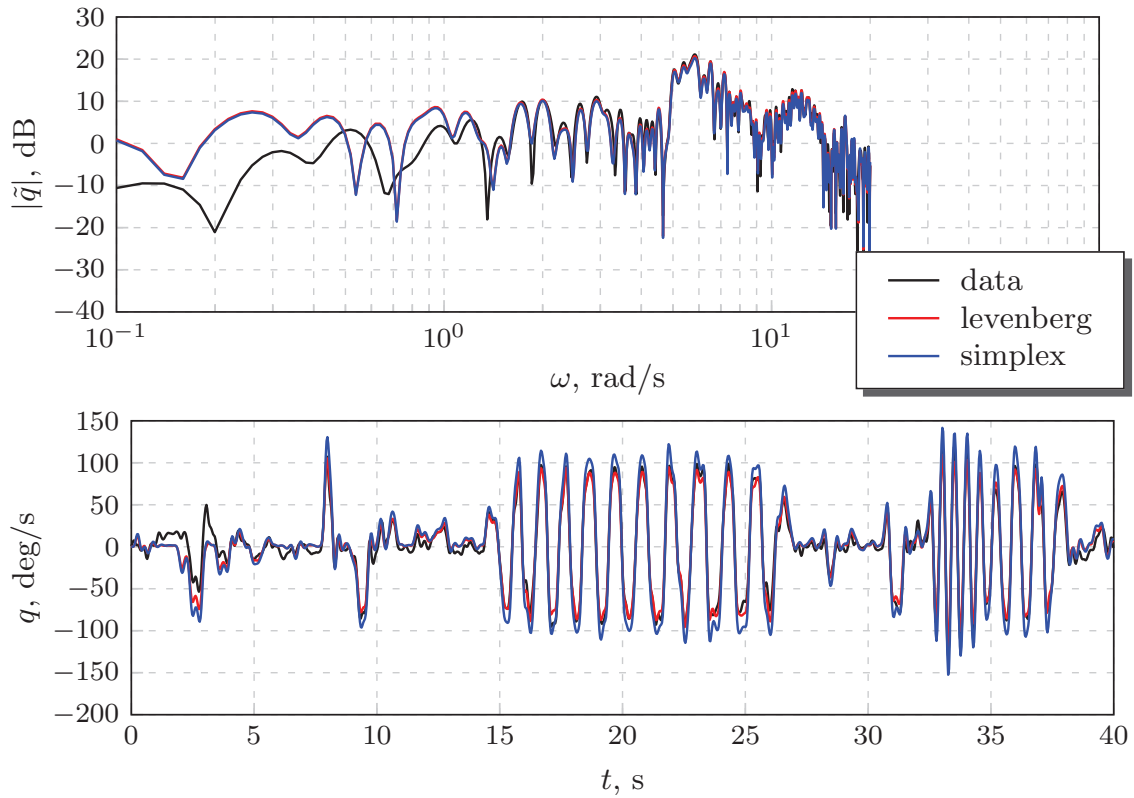


Figure 4.6: Identification results: OE method for short-period dynamics

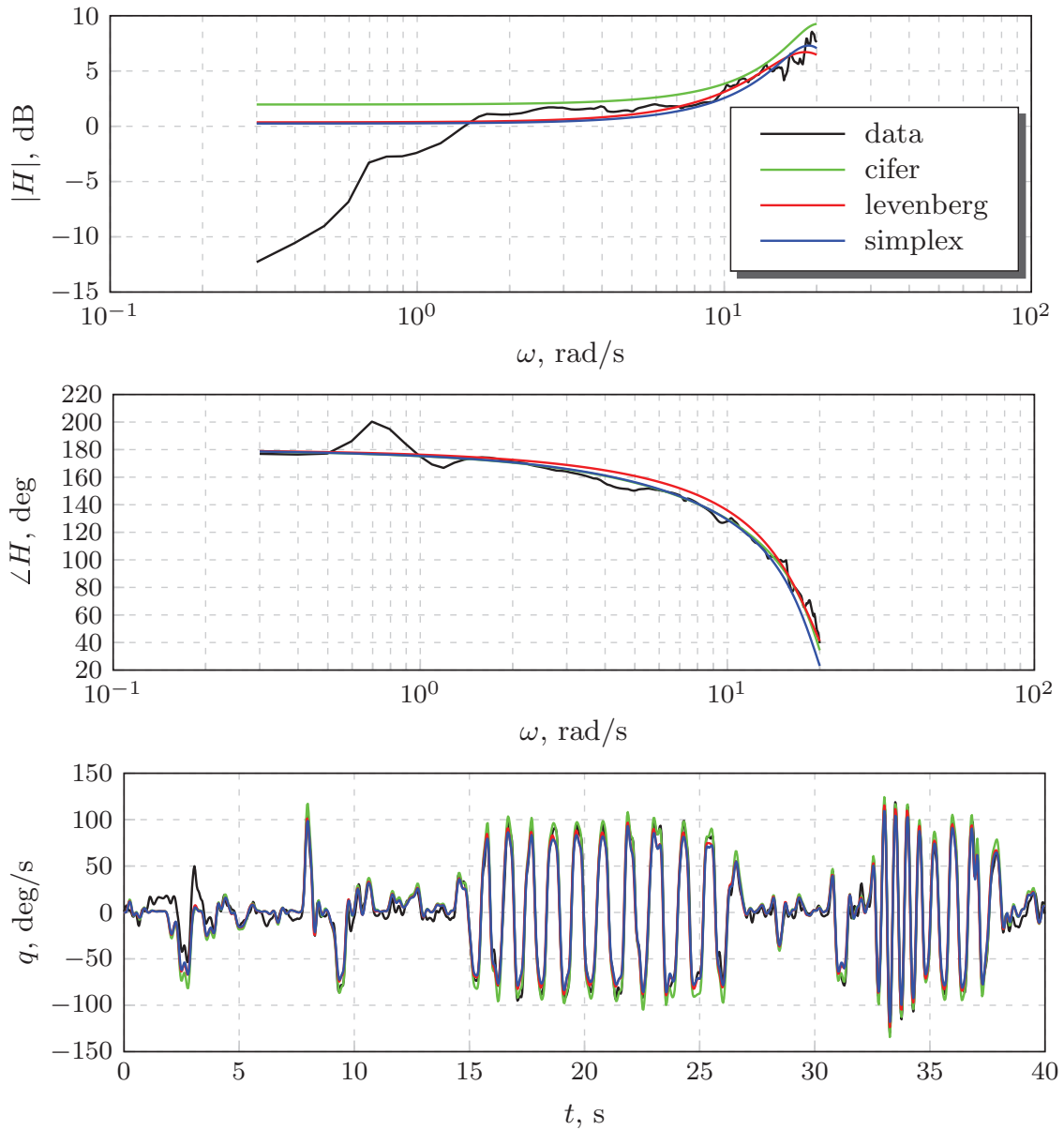


Figure 4.7: Identification results: FE method for short-period dynamics

4.6.2 Lateral Dynamics

The parameters to be estimated are b_0 , a_1 , a_0 , and τ from the transfer function given in Tables 4.1. For the Levenberg and Simplex solutions, only time delay τ is fixed during the iterations. It is initially set to its corresponding value from CIFER, but fine-tuned manually during multiple runs of the Matlab code. Analogous to the

longitudinal mode, Table 4.4 and 4.5 summarize the estimation results of the output-error and frequency-response-error methods, respectively. Also, Fig. 4.9 and Fig. 4.8 illustrate the results of these two methods in time and frequency domains.

Table 4.4: Identification results: OE method for roll dynamics

Symbols	Parameter Estimates	
	Levenberg	Simplex
b_0	491.00	391.40
a_1	9.44	9.90
a_0	436.21	380.00
τ	0.05	0.05
ζ	0.23	0.25
ω_n	20.89	19.49
J_{OE}	410.74	496.76

Table 4.5: Identification results: FE method for roll dynamics

Symbols	Parameter Estimates		
	Levenberg	Simplex	CIFER [®]
b_0	383.43	394.82	247.1
a_1	6.13	9.86	9.84
a_0	333.40	371.64	232.5
τ	0.07	0.05	0.01
ζ	0.17	0.26	0.32
ω_n	18.26	19.27	15.25
J_{FE}	66.72	132.86	147.73

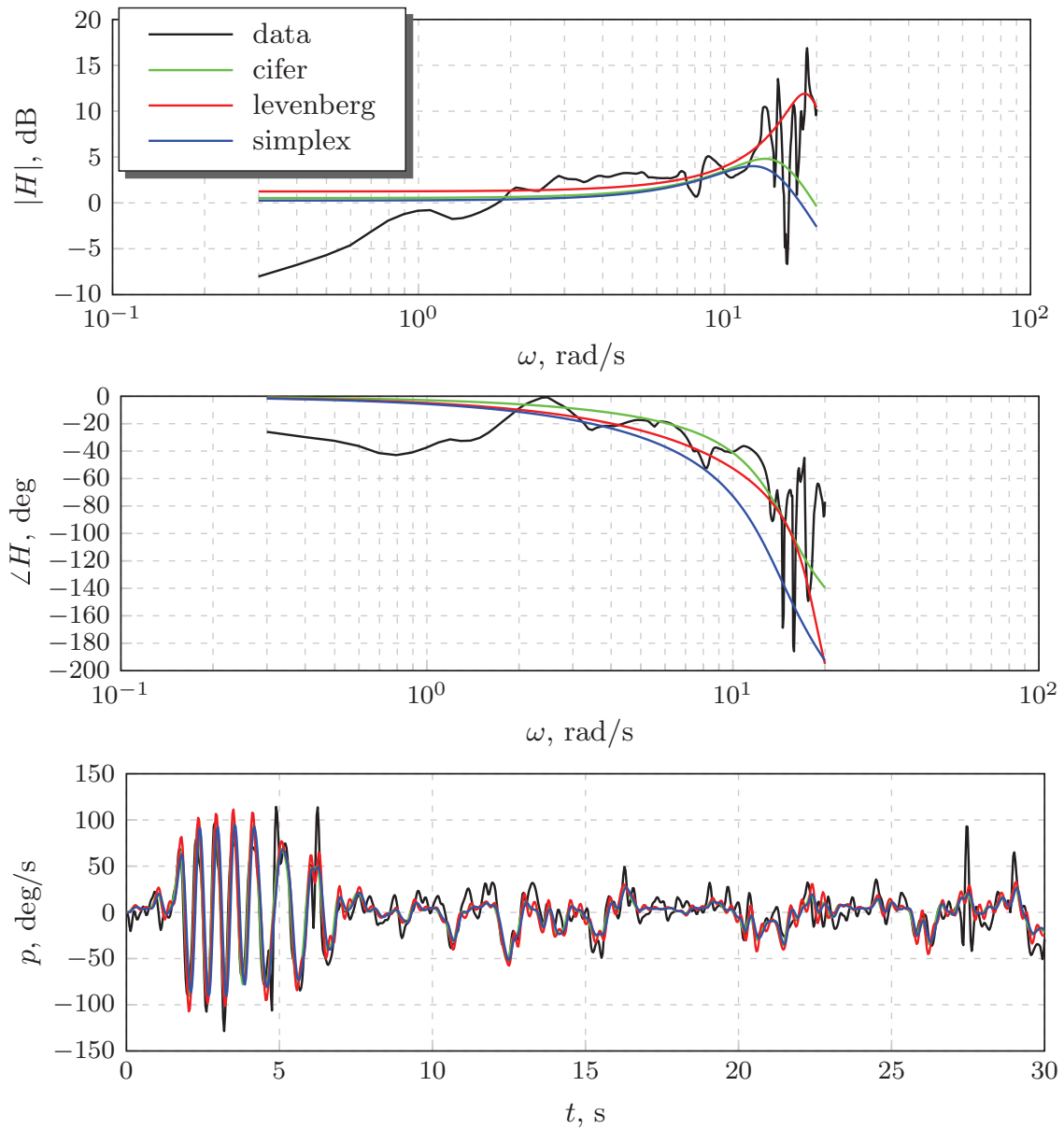


Figure 4.8: Identification results: FE method for roll dynamics

4.7 Analysis and Discussion

The accuracy of the estimation can be examined by evaluating the Cramer-Rao bound for each parameter, as given in equations (4.55) and (4.56). The Cramer-Rao bounds for the parameters which were kept free during the optimization are given

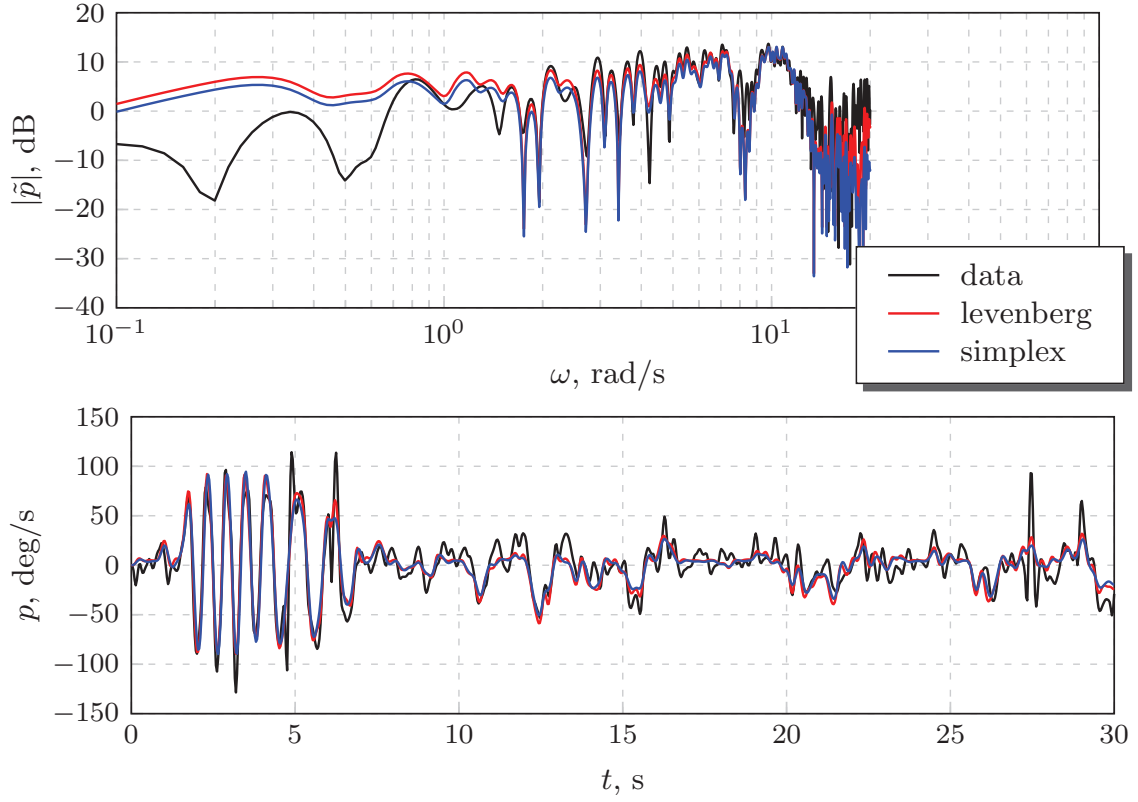


Figure 4.9: Identification results: OE method for roll dynamics

in Table 4.6 for the short-period and the roll dynamics. According to reference [12], a highly reliable model identification with proper predictive accuracy is achieved if the cost value and Cramer-Rao bounds agree with the following guidelines:

$$J_{FE} \leq 100 \quad (4.83)$$

$$CR_{FE} \leq 40\%. \quad (4.84)$$

It is also worth mentioning that due to the different definitions for the cost function of the output-error and the frequency-response-error methods (equations (4.40) and (4.42)), the resulting cost values, J_{OE} and J_{FE} , are incomparable. This also involves the Cramer-Rao bounds, CR_{OE} and CR_{FE} , as they result from the second-order gradient of the cost function according to equation (4.54).

Table 4.6: Cramer-Rao bound for short-period dynamics

Mode	Parameter	CR _{FE} %	CR _{OE} %
Pitch	b_1	36.709	0.018
	a_1	22.604	0.012
	a_0	4.046	0.032
Roll	b_0	48.049	0.297
	a_1	52.036	0.788
	a_0	39.835	0.263

Overall, the identified LOES models for pitch and roll dynamics are very accurate in mid and high frequencies, as can be seen in Figures 4.6 to 4.8. However, the LOES model prediction of the low-frequency longitudinal and lateral dynamics (lower than 0.8 rad/s for pitch, and 1 rad/s for roll motion) is relatively poor and not acceptable. Besides, in the identified LOES models for the short-period mode using OE and FE methods, the Levenberg solution gives a better fit with lower cost values (see Tables 4.2 and 4.3). This is also consistent with the identified LOES models for the roll dynamics (see Tables 4.4 and 4.5). Moreover, the LOES models for pitch and roll dynamics obtained from OE and FE methods are superior compared to the models identified using CIPHER transfer function identification package, as they have relatively lower cost values (see Tables 4.3 and 4.5).

From another point of view, the identified LOES model for the the longitudinal mode is more accurate compared to the lateral model. This is consistent for all methods and solutions, in other words:

$$(J_{FE})_{pitch} < (J_{FE})_{roll} \quad (4.85)$$

$$(J_{OE})_{pitch} < (J_{OE})_{roll} \quad (4.86)$$

$$(CR_{FE_i})_{pitch} < (CR_{FE_i})_{roll} \quad \forall i = 1, \dots, n_p \quad (4.87)$$

$$(CR_{OE_i})_{pitch} < (CR_{OE_i})_{roll} \quad \forall i = 1, \dots, n_p \quad (4.88)$$

where n is the number of parameters kept free during the estimation. The better results for longitudinal identified model can be essentially seen in the simpler longitudinal dynamics compared to the lateral dynamics which is highly coupled with directional motion. In other words, the second-order LOES model might not be sufficient for capturing the lateral dynamics completely. However, the most probable reason is the poor excitation of the roll dynamics as can be seen in spectral estimates of the lateral input presented and discussed in Section 3.5. These results can be further augmented if a new set of flight test data, which is richer in frequency content, is available [49].

From another point of view, the parameter estimates reflect a physically meaningful prediction of the Trex-700 longitudinal and lateral dynamics, which is in agreement with the identification results of R-50 small-scale helicopter presented in reference [16]. This can be seen in the calculated modal characteristics given in Tables 4.2 to 4.5. The modal characteristics of the longitudinal dynamics ($\omega_n = 19.75$ rad/s and $\zeta = 0.39$) shows a fast oscillatory moderately damped short-period mode. For the lateral dynamics, the modal characteristics ($\omega_n = 18.26$ rad/s and $\zeta = 0.17$) also reflect a relatively fast lightly damped roll mode. Among various identified model for each mode, the FE method with Levenberg solution gives the most accurate result. The final results for the LOES transfer functions of the longitudinal and lateral on-axis responses are presented in the following equations:

$$\frac{q}{\delta_{lon}} = \frac{-25.45s - 400.00}{s^2 + 15.28s + 390.19} e^{-0.08s} \quad (4.89)$$

$$\frac{p}{\delta_{lat}} = \frac{383.43}{s^2 + 6.13s + 333.40} e^{-0.07s}. \quad (4.90)$$

Chapter 5

Conclusion

Finding an accurate mathematical model for expressing aerodynamic behavior of small-scale aerial vehicles is a challenging task in model-based flight research. The lack of accuracy in conventional analytical models calls for the need to use alternative techniques for modeling these types of aircraft. System identification is considered as a reliable and less expensive substitute approach which provides highly accurate models in various forms, such as frequency-response, transfer function, state-space, or nonlinear models from measured flight data.

This thesis provided an overview of frequency-domain identification approaches, namely frequency-response and LOES methods, and their corresponding estimation and optimization techniques. It also shed some light on flight experiment design, and model structure determination as crucial prerequisites for a consistent model identification. The primary purpose of this work is developing an identification tool for rotary-wing UAVs which can automatically and efficiently interact with the flight simulation software available for the test platforms. The developed tool can be used as a groundwork for in-flight system identification applied to fault-tolerant and adaptive control. It can also optimize the control system design procedure by delivering more realistic models.

A Matlab-based tool is developed throughout this research. Real flight data have been used to verify the merit of the developed tool for identifying persistent and reliable models. This involved designing and conducting flight test for acquiring measurement input-output data of a test vehicle. The aircraft selected for this reason is a flybarless single-rotor R/C helicopter named Trex-700. The flight test is executed by MicroPilot in hover regime by exciting longitudinal and lateral cyclic controls using frequency sweep inputs. The resulting input-output pairs for pitch and roll motions are fed to the identification tool as well as CIPHER to obtain non-parametric and transfer function models of the aircraft. Accuracy metrics and results comparison depict an excellent match between CIPHER models and the models extracted using the SID tool in almost entire frequency range of interest. This demonstrates the capability of the developed system identification tool for estimating accurate models for unmanned helicopters.

One future direction of this research can be considered as extending the current framework to MIMO state-space model identification. This developed code can be also used for development and application of new theory and methodologies in system identification. Also, an important extension of this research is considered as in-flight identification which requires employing non-iterative methods which are also capable of state estimation, such as filter-based recursive approaches. In another future direction, the model identified for the test vehicle can be further analyzed and validated by conducting additional flight experiments and acquiring more measurements in order to include other dynamic modes such as heave and yaw. Also, the doublet inputs designed in Chapter 2 can be utilized in future flight test to collect data for time-domain model validation. Finally, in the frequency-response identification, improved spectral estimates can be achieved if a nonlinear optimization is used for the composite windowing technique.

Bibliography

- [1] B. Mettler, M. B. Tischler, and T. Kanade, “System identification of small-size unmanned helicopter dynamics,” in *The American Helicopter Society 55th Forum*, (Montreal, Quebec, Canada), May 1999.
- [2] E. B. Stear *et al.*, “System identification for integrated aircraft development and flight testing,” in *Proceedings of the RTO Systems Concepts and Integration Panel (SCI) Symposium*, (Madrid, Spain), 1998.
- [3] L. R. Rabiner, R. W. Schafer, and C. M. Rader, “The chirp z-transform algorithm and its application,” *Bell System Technical Journal*, vol. 48, no. 5, pp. 1249–92.
- [4] G. D. Padfield, *Helicopter flight dynamics: The theory and application of flying qualities and simulation modelling*. Blackwell Publication Ltd., 2nd ed., 2007.
- [5] W. H. Press, B. P. Flannery, S. A. Teukolsky, and W. T. Vetterling, *Numerical recipes in FORTRAN 77: The art of scientific computing*. Cambridge University Press, 2nd ed., 1992.
- [6] J. L. Crassidis and J. L. Junkins, *Optimal estimation of dynamic systems*. CRC press, 2011.

- [7] C. R. Theodore, M. B. Tischler, and J. D. Colbourne, “Rapid frequency-domain modeling methods for unmanned aerial vehicle flight control applications,” *Journal of Aircraft*, vol. 41, no. 4, pp. 735–743, 2004.
- [8] P. G. Hamel and J. Kaletka, “Advances in rotorcraft system identification,” *Progress in Aerospace Sciences*, vol. 33, no. 3-4, pp. 259–284, 1997.
- [9] B. F. Mettler, *Modeling small-scale unmanned rotorcraft for advanced flight control design*. PhD thesis, 2001.
- [10] V. Klein and E. A. Morelli, *Aircraft system identification: theory and practice*. American Institute of Aeronautics and Astronautics, 2006.
- [11] G. Chowdhary and R. Jategaonkar, “Aerodynamic parameter estimation from flight data applying extended and unscented kalman filter,” *Aerospace Science and Technology*, vol. 14, no. 2, pp. 106–117, 2010.
- [12] M. B. Tischler and R. K. Rempfle, *Aircraft and rotorcraft system identification: engineering methods with flight-test examples*. American Institute of Aeronautics and Astronautics, 2006.
- [13] E. A. Morelli, “System identification programs for aircraft (SIDPAC),” in *AIAA Atmospheric Flight Mechanics Conference*, (Monterey, CA, USA), August 2002.
- [14] B. Mettler, T. Kanade, and M. B. Tischler, “System identification modeling of a model-scale helicopter,” Tech. Rep. CMU-RI-TR-00-03, 2000.
- [15] B. Mettler, M. B. Tischler, and T. Kanade, “System identification modeling of a small-scale unmanned rotorcraft for flight control design,” *Journal of the American Helicopter Society*, vol. 47, no. 1, pp. 50–63.
- [16] B. Mettler, *Identification modeling and characteristics of miniature rotorcraft*. Kluwer Academic Publishers, 2003.

- [17] G. Cai, B. M. Chen, K. Peng, M. Dong, and T. H. Lee, "Modeling and control system design for a UAV helicopter," in *Proceedings of the 14th Mediterranean Conference on Control and Automation*, (Piscataway, NJ, USA), June 2006.
- [18] J. Grauer, J. Conroy, J. H. J., J. Humbert, and D. Pines, "System identification of a miniature helicopter," *Journal of Aircraft*, vol. 46, no. 4, pp. 1260–1269, 2009.
- [19] J. K. Conroy, J. S. Humbert, and D. J. Pines, "Technical note: System identification of a rotary-wing micro air vehicle," *Journal of the American Helicopter Society*, vol. 56, no. 2, p. 25001, 2011.
- [20] W. Yuan and J. Katupitiya, "A two-stage method for the parametric identification of scale-model helicopter dynamics," in *AIAA Atmospheric Flight Mechanics Conference*, (Minneapolis, MN, USA), August 2012.
- [21] E. R. Ulrich, J. S. Humbert, and D. J. Pines, "Pitch and heave control of robotic Samara micro air vehicles," *Journal of Aircraft*, vol. 47, no. 4, pp. 1290–9, 2010.
- [22] S. Kim and D. Tilbury, "Mathematical modeling and experimental identification of an unmanned helicopter robot with flybar dynamics," *Journal of Robotic Systems*, vol. 21, no. 3, pp. 95–116.
- [23] A. Al-Radaideh, A. A. Jhemi, and M. Al-Jarrah, "System identification of the Joker-3 unmanned helicopter," in *AIAA Modeling and Simulation Technologies Conference*, (Minneapolis, MN, USA), August 2012.
- [24] G. Cai, B. M. Chen, K. Peng, M. Dong, and T. H. Lee, "Modeling and control of the yaw channel of a UAV helicopter," *IEEE Transactions on Industrial Electronics*, vol. 55, no. 9, pp. 3426–34, 2008.
- [25] R. V. Jategaonkar, "Flight vehicle system identification in time domain: Short course (tutorial) notes," Tech. Rep. NASA-TM-89428, 2009.

- [26] A. Wypyszynski, “Flight testing of small remotely piloted aircraft for system identification,” Master’s thesis, 2009.
- [27] J. N. Williams, J. A. Ham, and M. B. Tishler, “Flight test manual: rotorcraft frequency domain flight testing,” Tech. Rep. 93-14, 1995.
- [28] R. Jategaonkar, *Flight vehicle system identification: A time domain methodology*. American Institute of Aeronautics and Astronautics, 2006.
- [29] E. A. Morelli, “Low-order equivalent system identification for the Tu-144LL supersonic transport aircraft,” *Journal of Guidance, Control, and Dynamics*, vol. 26, no. 2, pp. 354–362, 2003.
- [30] E. A. Morelli, “Identification of low order equivalent system models from flight test data,” Tech. Rep. 210117, 2000.
- [31] Align Corporation Limited, Taiwan, *Trex-700E Instruction Manual*, 2012.
- [32] C. M. Close, D. K. Frederick, and J. C. Newell, *Modeling and analysis of dynamic systems*. Wiley, 3rd ed., 2002.
- [33] E. Morelli, “High accuracy evaluation of the finite fourier transform using sampled data,” Tech. Rep. NASA-TM-110340, 1997.
- [34] J. S. Bendat and A. G. Piersol, *Random data: Analysis and measurement procedures*. Wiley, 4th ed., 2010.
- [35] J. Antoni and J. Schoukens, “FRF measurements with the weighted overlapped segment averaging technique,” in *IFAC Symposium Modelling, Identification and Signal Processing (SYSID 2006) Identification and System Parameter Estimation*, (Amsterdam, Netherlands), 2006.
- [36] A. Bramwell, G. Done, and D. Balmford, *Bramwell’s Helicopter Dynamics*. American Institute of Aeronautics and Astronautics, 2001.

- [37] W. Johnson, *Helicopter Theory*. Dover Publications, 1994.
- [38] A. Dorobantu, *Test Platforms for Model-Based Flight Research*. PhD thesis, 2013.
- [39] M. B. Tischler and M. G. Cauffman, “Frequency-response method for rotorcraft system identification: Flight applications to BO 105 coupled rotor/fuselage dynamics,” *Journal of the American Helicopter Society*, vol. 37, no. 3, pp. 3–17.
- [40] R. Nelson, *Flight stability and automatic control*. McGraw-Hill, 1998.
- [41] W. Duncan, *Principles of Control and Stability of Aircraft*. Cambridge University Press, 2003.
- [42] I. A. Raptis, *Linear and nonlinear control of unmanned rotorcraft*. PhD thesis, 2010.
- [43] Y. Ben, *Development of a miniature low-cost UAV helicopter autopilot platform and formation flight control of UAV teams*. PhD thesis, 2010.
- [44] S. Bhandari, *Flight validated high-order models of UAV helicopter dynamics in hover and forward flight using analytical and parameter identification techniques*. PhD thesis, 2007.
- [45] R. L. W. Choi, C. E. Hann, and X. Chen, “Minimal models to capture the dynamics of a rotary unmanned aerial vehicle,” *Journal of Intelligent and Robotic Systems: Theory and Applications*, pp. 1–25.
- [46] J. Wright and J. Cooper, *Introduction to Aircraft Aeroelasticity and Loads*. Wiley, 2008.
- [47] T. Takahama and S. Sakai, “Constrained optimization by applying the α constrained method to the nonlinear simplex method with mutations,” *IEEE Transactions on Evolutionary Computation*, vol. 9, no. 5, pp. 437–451.

- [48] J. A. Nelder and R. Mead, “A Simplex method for function minimization,” *The Computer Journal*, vol. 7, no. 4, pp. 308–313.
- [49] M. Mohajerani, H. Bolandhemmat, Y. Zhang, and H. Loewen, “Identification of low order equivalent transfer function model of Trex-700E helicopter from flight test data,” in *AIAA Modeling and Simulation Technologies Conference*, (Reston, VA, USA), 2014.